On the characteristics of vortex filaments in isotropic turbulence

By JAVIER JIMÉNEZ[1,2] and ALAN A. WRAY[3]

[1] School of Aeronautics, U. Politécnica, 28040 Madrid, Spain

[2] Centre for Turbulent Research, Stanford U. Stanford, CA 94305, USA

[3] NASA Ames Research Centre, Moffett Field, CA 94035, USA

The statistical properties of the strong coherent vortices observed in numerical simulations of isotropic turbulence are studied. When compiled at axial vorticity levels $\omega/\omega' \sim Re_\lambda^{1/2}$, where ω' is the r.m.s. vorticity magnitude for the flow as a whole, they have radii of the order of the Kolmogorov scale and internal velocity differences of the order of the r.m.s. velocity of the flow u'. Theoretical arguments are given to explain these scalings. It is shown that the filaments are inhomogeneous Burgers' vortices driven by an axial stretching which behaves like the strain fluctuations of the background flow. It is suggested that they are the strongest members in a class of coherent objects, the weakest of which have radii of the order of the Taylor microscale, and indirect evidence is presented that they are unstable. A model is proposed in which this instability leads to a cascade of coherent filaments whose radii are below the dissipative scale of the flow as a whole. A family of such cascades separates the self-similar inertial range from the dissipative limit. At the vorticity level given above, the filaments occupy a volume fraction which scales as Re_λ^{-2}, and their total length increases as $O(Re_\lambda)$. The length of individual filaments scales as the integral length of the flow, but there is a shorter internal length of the order of the Taylor microscale.

1. Introduction

This paper is devoted to the analysis of the coherent vortices that are known to exist among the small scales of many turbulent flows, and is a continuation of the previous one by Jiménez *et al.* (1993, referred to hereafter as JWSR). That paper was devoted to the statistical properties of small-scale vorticity, and paid some attention to its structural aspects. It had been found at the time that small-scale vorticity was organized in the form of vortex filaments, and one of the goals of the paper was the identification of scaling laws for their properties. The filaments had first been found in numerical simulations by Siggia (1981), although they had been suggested earlier from laboratory experiments by Kuo & Corrsin (1972). Several numerical and experimental investigations had confirmed their existence (see JWSR for a list of references up to 1992), but it was in JWSR that they were first studied over a range of Reynolds numbers wide enough to establish their scaling properties. This led to contradictions with the assumptions of some of the previous investigators, and to a number of theoretical problems.

There were three main outstanding issues. In the first place it was found that the radius of the vortices was proportional to the Kolmogorov microscale of the flow η,

while most previous work had favoured radii of the order of the Taylor microscale λ. At the low Reynolds numbers of the simulations both scales are difficult to tell apart, but they vary in different ways with the Reynolds number, and the scaling found in JWSR was unequivocal. This raised a theoretical question, since these radii implied that the vortices were being stretched by strains of the order of the r.m.s. flow vorticity, ω', and it was difficult to understand how such strong strains could be coherent over distances of the order of the length of the vortices, which were known to be much longer than the Kolmogorov scale.

The second problem was the intensity of the vortices, which was found to require azimuthal velocities of the order of the large-scale r.m.s. velocity of the flow. Since the latter is a property of the large scales of the flow, while the former occur across distances of the order of the Kolmogorov scale, it was difficult to understand how one could influence the other.

Finally, it was noted in JWSR that the two previous scalings implied that the internal Reynolds number of the vortices was high, and increased with the Reynolds number of the flow, suggesting that they might be transitional phenomena associated with low Reynolds number turbulence, and that they should eventually become internally unstable and disappear when the Reynolds number of the flow was high enough.

These and other inconsistencies have motivated a lot of work since that time. The formation of the filaments was studied by Vincent & Meneguzzi (1994) and by Passot *et al.* (1995), who concluded that they were formed by instabilities of existing vortex sheets. The filaments themselves were studied experimentally by Cadot, Douday & Couder (1995) and by Abry *et al.* (1994) by analysing the low pressures in their cores. Belin *et al.* (1996) confirmed the presence of velocity fluctuations of the magnitude and length scale mentioned above at Reynolds number much higher than those in simulations ($Re_\lambda = 700$), and the same was done using optical techniques by Noullez *et al.* (1997). Although these are one-point one-component velocity measurements from which it is difficult to conclude the geometry of the structures, they are at least consistent with vortex filaments which scale in the same way as in the simulations. Y. Malecot (1997, private communication) analysed two-component velocity measurements from a jet at $Re_\lambda = 800$, and found events consistent with filaments with radii and velocities very similar to those of the simulations. The constraints on a two-component signal are much stronger than those on a one-component one, and there is little doubt that the structures found in that case are vortices. New simulations at Reynolds numbers comparable to those in JWSR were done by Tanahashi, Miyauchi & Ikeda (1997) in isotropic turbulence, and by Tanahashi, Miyauchi & Matsuoka (1997) in a turbulent shear layer. Although their vortex identification technique is very different from that in JWSR their results agree with the older ones within a few percent. A compilation of the results obtained to date for the vortex scalings can be found in Jiménez (1997). An important theoretical advance was achieved by Verzicco, Jiménez & Orlandi (1993, referred to hereafter as VJO), who studied the dynamics of vortices subject to non-uniform, spatially periodic, strains, and were able to suggest explanations for the velocity and radius scalings mentioned above. The same group has extended their conclusions to more general stretching laws which better approximate those found in turbulence (Verzicco & Jiménez 1997).

In spite of all this work, which broadly confirms the results of JWSR, the data in that paper still include the highest Reynolds number simulations available for the study of the vortex filaments. The purpose of the present paper is to use them, slightly extended, to address the questions posed at the beginning of this introduction,

	Re_λ	N	L_ϵ	L/L_ϵ	t/T	R/η	R/R_b	ω_0/ω_f	u_0/u'	N_f	N_w
——	37	64	1.8	1.09	54.2	4.8	0.92	0.34	0.99	6	174
- - - -	62	128	2.2	0.80	9.3	4.9	0.94	0.31	0.91	6	357
········	95	256	2.0	0.72	8.2	4.8	0.95	0.30	0.86	4	396
—·—	142	384	2.4	0.73	5.9	4.9	1.01	0.30	0.86	5	344
—··—	168	512	2.4	0.69	5.1	4.8	1.03	0.33	0.92	2	122
—○—	163	512	2.2	0.69	7.1	4.8	1.05	0.35	0.99	1	58
△	62	512	0.36	1.31	—	4.9	0.82	0.42	1.21	1	159

TABLE 1. Numerical and flow parameters for the simulations analysed in this paper. t/T is the total run time in eddy-turnover units, L is the integral scale and $L_\epsilon = u'^3/\epsilon$ is the eddy-dissipation scale. The size of the computational box is 2π. The next-to-last line is the 512^3 data set which has been discarded in most cases, as explained in the text. The last one is the decaying field. The last six columns refer to filament tracking results discussed in §4. N_f is the number of fields used for tracking, and N_w is the number of individual filaments identified.

including the theoretical suggestions in VJO, as well as other open questions related to the structure of the filaments. Foremost among those is the question of the relative importance of the filaments in the flow as a whole, and their relation, if any, with the intermittency properties of turbulence. On this last subject two recent surveys have to be mentioned: the phenomenological one by Sreenivasan & Antonia (1997) and the more theoretical book by Frisch (1995). Two earlier publications by our group constitute interim reports on the results in the present paper (Jiménez & Wray 1994*a, b*).

The organization of the paper is as follows. In the next section the numerical simulations are described, followed in §3 by a description of the details of the vortex tracking procedure. The statistics obtained on the filaments are described in §4, including local properties, filament lengths and relative volume fractions. A discussion follows, including the indirect evidence for the existence of a coherent cascade beyond the Kolmogorov limit, and its interpretation in relation to the multifractal model of turbulence. A subsection discusses possible experimental checks of the proposed model. The paper ends by offering conclusions and a list of open problems.

2. Numerical simulations

The simulations used in this paper are essentially those in JWSR, but a new intermediate Reynolds number has been added, and most of them have been continued for longer times to improve the statistics. The spectral numerical scheme (Rogallo 1981) and other parameters are described in JWSR, which should be consulted for the detailed definitions of the different quantities (Batchelor 1953). With the single exception described below, all the simulations are forced at the wavenumbers for which $k = |\boldsymbol{k}| \leqslant 2.5$ to achieve a statistically stationary state with a fixed value for $k_{max}\eta$. The two lower Reynolds numbers have been repeated at doubled resolution to check for possible scaling artifacts. All the simulations (at $k_{max}\eta = 2$) are summarized in table 1.

The limited range of forced wavenumbers maximizes the attainable Reynolds number, but introduces a large variability in the statistics, with a characteristic time scale of the order of the eddy-turnover time. For example the value of Re_λ varies almost 10% within a given simulation. It follows from standard Kolmogorov theory that the smaller flow scales vary faster than the larger ones, while the cost of running

a simulation increases with the fourth power of the linear size of the computational grid, mostly due to the modes needed to represent the smallest scales. To save computational resources most flows were run for long times at $k_{max}\eta = 1$, and the resolution was doubled at intervals of one or two turnover times. The flow was then run at $k_{max}\eta = 2$ for 0.3–0.5 turnover times, and the final field was stored for analysis. That the evolution of the large scales was only weakly affected by this procedure was tested independently in a pair of simultaneous computations on 128^3 and 256^3 grids. The evolution times given in the table are low-resolution ones. The number of fields stored and analysed varies from about 10 for the lower Reynolds numbers to 3 for the highest one.

In the latter case, the small number of fields results in serious statistical uncertainties; two of the fields agree with each other and are in line with the scalings suggested by the other Reynolds numbers, but the third is substantially more intermittent. The tails of the p.d.f.s of its velocity gradients are almost an order of magnitude larger at the 10^{-7} level than the average of the two other fields. Note that this probability level corresponds to the difference of finding high activity in a region of 2^3 or 4^3 grid points in a 512^3 field. The rest of this paper deals with events at the 10^{-3}–10^{-4} probability level. A comparable violent event is observed in the $Re_\lambda = 64$ computation, where it has a duration of a fraction of one turnover time in a simulation of over 50. Its effects can be seen as a bulge in the tail of the probability distribution of the vorticity in figure 7. These events probably represent an intermittency class which occurs too seldom to be studied with our limited statistical samples. If we assume that the small scales are independent of each other when their separation is larger than about 10η, which is the wavelength beyond which the velocity spectrum looses its power-law behaviour, our samples are roughly equivalent to one-dimensional signals with lengths between $10^5\eta$ and $10^6\eta$.

The anomalous 512^3 field has not been used in most of the statistics presented in this paper, since it would probably bias rather than complete them, but it has been included as an independent case in those figures in which it differs substantially from the mean, to give an idea of the uncertainty in the present conclusions.

One decaying field is included in our analysis to isolate possible spurious effects of the forcing on the properties of the filaments. It is a simulation at somewhat reduced resolution which was started from an uncorrelated random field at $Re_\lambda \approx 950$ and allowed to decay (Wray 1997). By the time it reached $Re_\lambda = 62$, its resolution had improved to $k_{max}\eta = 1.4$ and it could be compared to our forced case at the same Reynolds number.

3. Vortex tracking

The procedure for tracking the axes of the vortex filaments is described in the appendix to JWSR. Briefly the algorithm follows lines along which the vorticity magnitude has a local maximum on the $(3 \times 3$ grid points) normal plane, and computes a local radial distribution of the azimuthally averaged axial vorticity, fitting it to

$$\omega = \omega_0 \exp(-r^2/R^2). \tag{3.1}$$

Figure 1(*a*) presents probability distributions for the relative approximation errors. It was shown by Jiménez & Wray (1994*a*) that the vortex filaments identified in this way are subject to axial compression along a substantial percentage of their axis, and it is of interest whether the Gaussian model, which is normally associated with
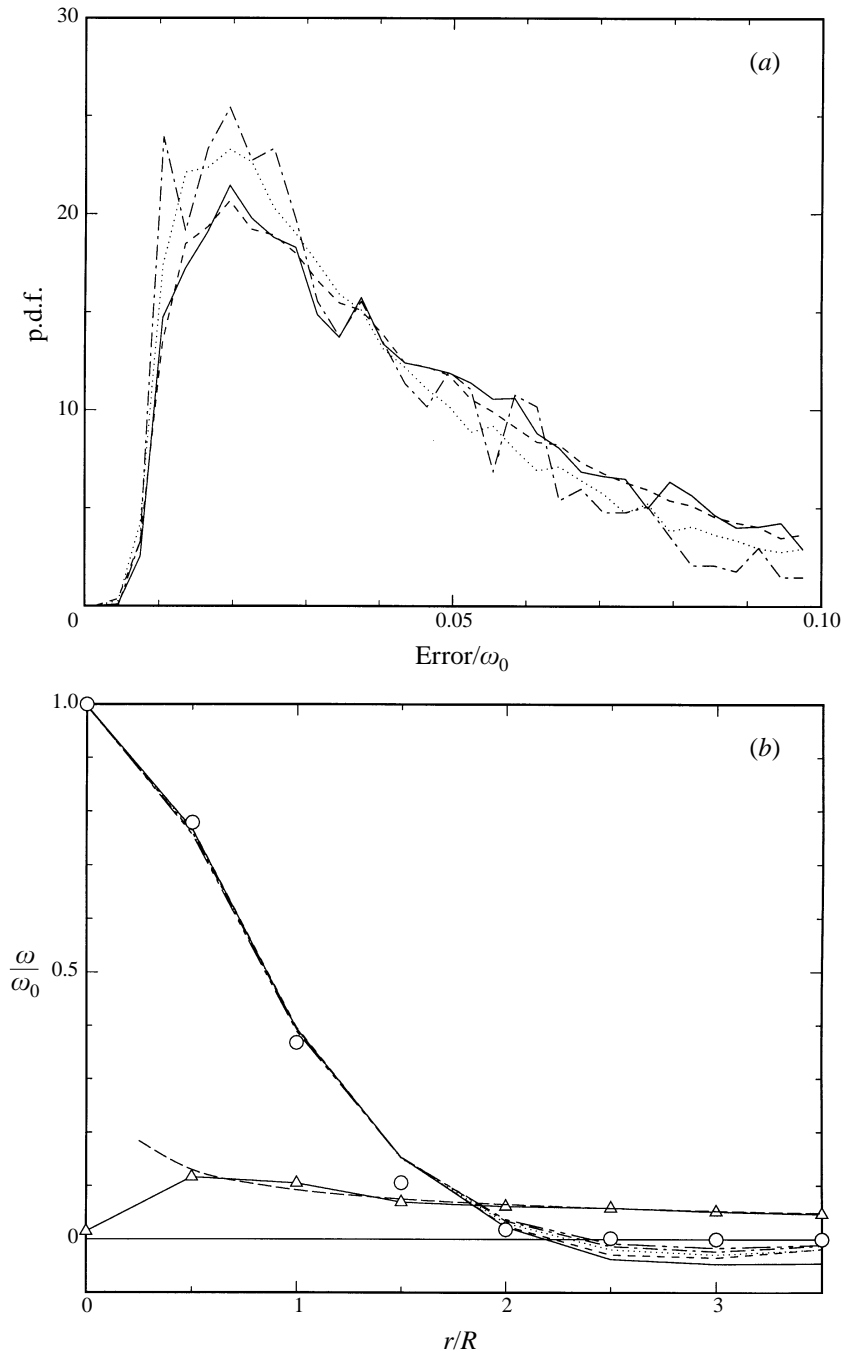
FIGURE 1. (*a*) Distribution of the r.m.s approximation error of the Gaussian model for the radial vorticity profile, computed inside a circle of radius $2R$, and normalized with the local ω_0. ——— , $Re_\lambda = 37$; – – – – , $Re_\lambda = 142$; —·— and ······· are distributions for the same Reynolds numbers, but only for axially compressed points. (*b*) Mean axial vorticity profile for the filaments, as a function of the Reynolds number, when each axial location is normalized with its local radius and central vorticity. Lines as in table 1. The circles are the Gaussian profile. —△— , standard deviation with respect to the mean, averaged over all Reynolds numbers. The dashed line which closely matches the standard deviation is (3.3).

axially strained vortices, can also be applied at those points. In the figure we have included the error distributions for the axially compressed points, in addition to those computed over the full filament, and it is seen that the model is still adequate for them. Corresponding to these low errors, the radial profile of axial vorticity, when averaged along the filaments, fits well the Gaussian assumption for all the Reynolds numbers in our simulations, as shown in figure 1(*b*). The figure also gives the standard deviation of individual profiles with respect to their axial mean.

Note that the foregoing discussion refers to the azimuthally averaged vorticity profiles. Individual sections of the filaments have larger local deviations from the Gaussian profile, and there is no implication in our data that the filaments are either exactly Gaussian or axisymmetric. In fact, since it follows from much of the evidence in this and in previous papers that filaments are especially intense instances of the general vorticity fluctuations, it should be expected that the magnitude of the local fluctuations with respect to the mean has a standard deviation of the order of ω' which, for $Re_\lambda \approx 100$, is of the order (see JWSR and figure 3*c*)

$$\omega' \approx 4Re_\lambda^{-1/2}\omega_0 \approx 0.4\,\omega_0. \tag{3.2}$$

This is especially true of the outer part of the profiles in figure 1, beyond $r \approx R$, where the average vorticity falls below ω' and the filaments merge into the general turbulent background. Fluctuations of this order can be seen in the vorticity trace across a filament shown in figure 17 of Vincent & Meneguzzi (1991), even though it is easy to check that the structure itself, which is about three times more intense, is well approximated by a Gaussian.

Azimuthal averaging smooths these fluctuations over $2\pi r/\Delta x$ points, where $\Delta x \approx 1.5\eta$ is the spacing of the collocation points, and the expected standard deviation of the azimuthally averaged profiles with respect to their global mean is

$$\frac{\Delta\omega}{\omega_0} \approx 4(2\pi Re_\lambda r/\Delta x)^{-1/2}. \tag{3.3}$$

This estimate has been included in figure 1(*b*), and agrees well with the observations.

Note that filaments can only be expected to be coherent at those locations in which $\omega_0 > \omega'$. As the Reynolds number decreases, the background fluctuations become of the same order as the maximum expected vorticity in the filaments, and the latter lose their individuality. It follows from (3.2) that this occurs approximately for $Re_\lambda < 30$, and experiments below this limit (e.g. Vassilicos & Brasseur 1996) are probably not relevant to the structures analysed here.

In our analysis, points at which the relative error is larger than 0.1 are discarded during postprocessing. So are points at which no solution exists to the fitting equations or where the computed radius is too large ($> 30\eta$), as well as those belonging to filaments which are shorter than an arbitrary limit of 20 grid points. All these procedures account for the loss of between 20% and 30% of the points originally identified by the tracker, of which 8%–12% are rejected due to large fitting errors, and the rest mostly in the form of short filaments. In addition, after all the filaments have been processed and assigned a radius, it is occasionally found that the tracker has identified the outer part of some of them as independent weaker structures, which are discarded. The percentage of points lost in this way ranges from less than 2% at the highest Reynolds number, where strong filaments are clearly differentiated from each other and from the background, to almost 40% at the lowest one. Statistics obtained over the remaining sample of filament axes are presented below, but one consideration must first be explained.
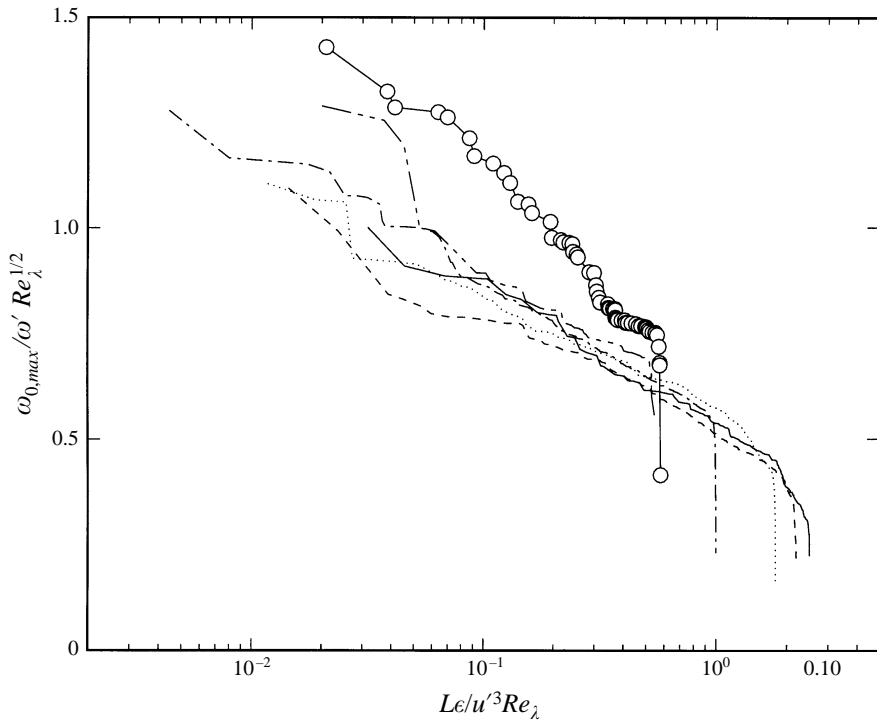
FIGURE 2. Maximum axial vorticity for individual filaments, as a function of the accumulated filament length, counted from the beginning of the tracking algorithm. Lines as in table 1.

In the implementation used in this paper the tracking algorithm runs for whichever is the longest allowable time at the particular computer in which the simulation resides, and there is no provision for the search to be restarted. Since the simulations at the different Reynolds numbers generate files of very different sizes, this procedure implies a more thorough search for the lower Reynolds numbers than for the higher ones, and that difference cannot be fully compensated by varying the search time.

The question is of some importance because there does not seem to be a natural definition for which vorticity structures should be considered as 'intense', besides being stronger than ω'. The tracking algorithm naturally orders filaments in terms of the highest vorticity found anywhere along their axes, with the most intense ones being found first, as shown in figure 2, which displays the maximum vorticity within each individual filaments as a function of the filament length accumulated since the beginning of the search. The statistics obtained from a short search are therefore different from those obtained from a longer one.

The effect on the statistics is not as severe as it appears at first sight, both because the vorticity along each filament is not uniform and its statistics therefore reflect part of the vorticity distribution over the whole sample (JWSR), and because the dependence of the maximum vorticity is only logarithmic on the accumulated length, but the bias is real and should be kept in mind when considering the statistics below. The question of which percentage of the filaments is represented in each sample will be discussed below, when we consider the volume filled by the intermittent vorticity.
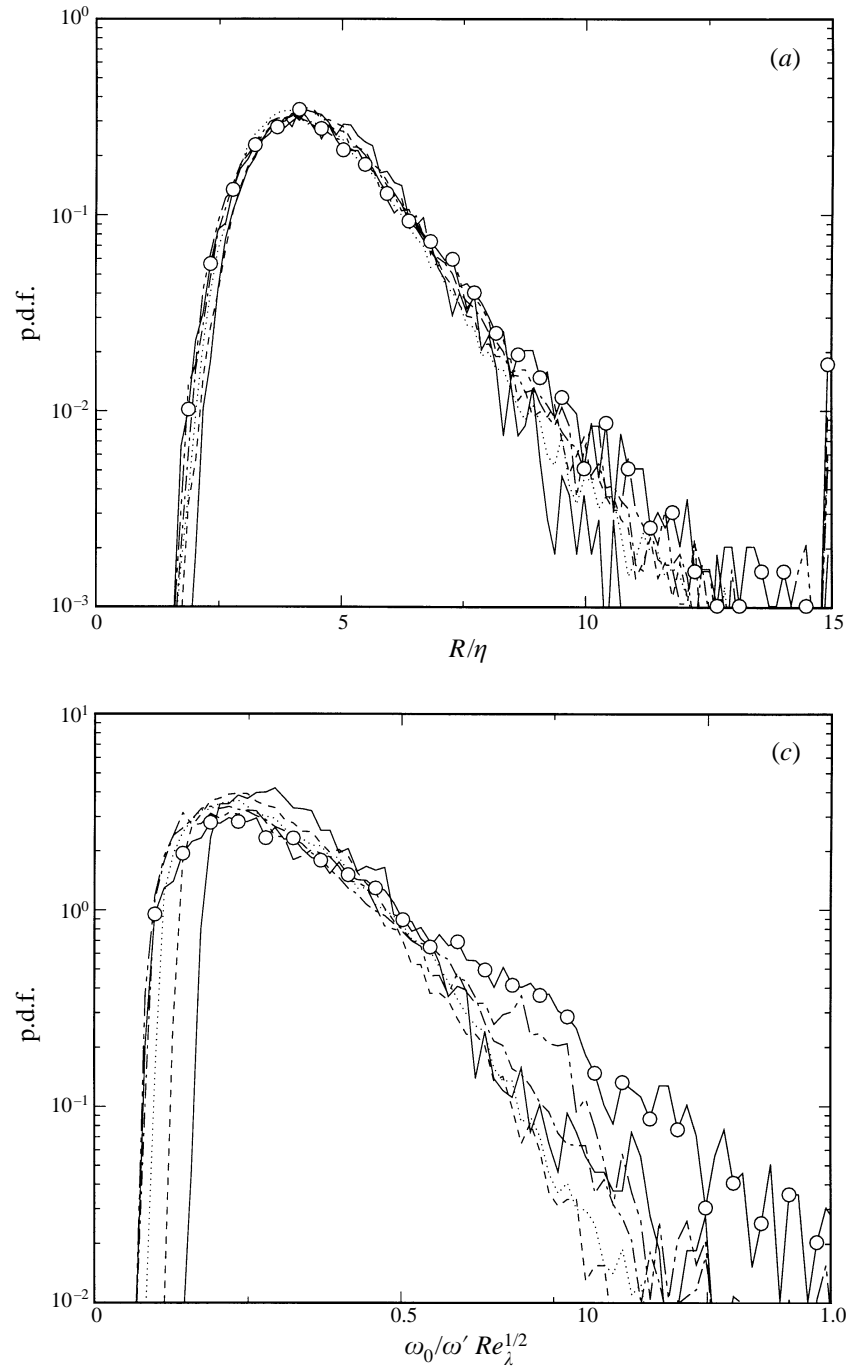
FIGURE 3 (*a,c*). For caption see facing page.

4. Statistical properties of the filaments

4.1. *Local properties*

At each point along the detected filaments the tracker computes a local radius R, a maximum vorticity magnitude $\omega_0 = |\boldsymbol{\omega}|$, and an axial stretching $\sigma_0 = \boldsymbol{\omega}_0 \cdot \mathbf{S} \cdot \boldsymbol{\omega}_0/\omega_0^2$,
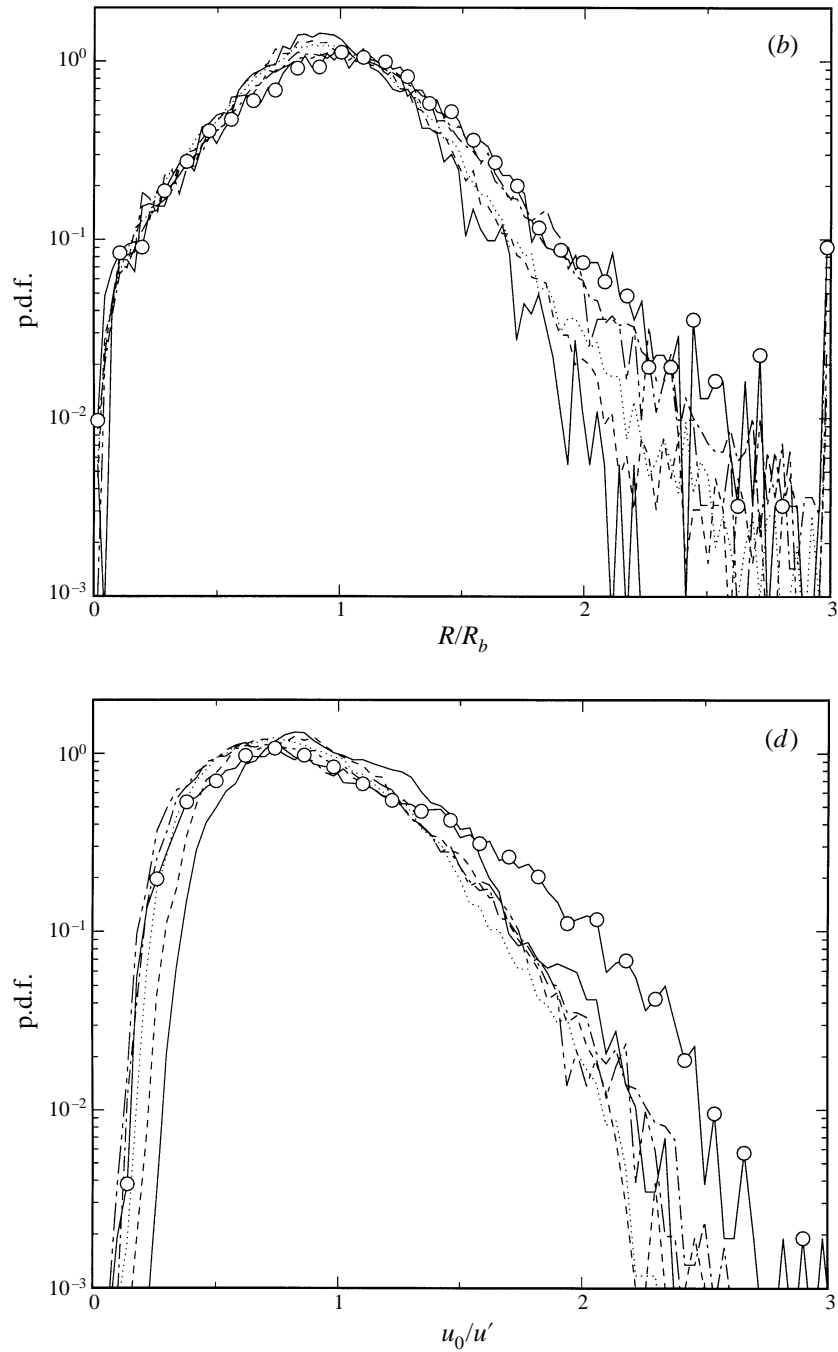
FIGURE 3. P.d.f.s of filament properties. (*a*) Radius normalized with the Kolmogorov scale. (*b*) Radius normalized with the local Burgers' radius. (*c*) Maximum axial vorticity. (*d*) Maximum azimuthal velocity.

where S is the rate of strain tensor. Assuming that the vorticity profile is Gaussian the local maximum azimuthal velocity is estimated as $u_0 = 0.319\,\omega_0 R$. The p.d.f.s of these quantities are shown in figure 3. They have been normalized in the way suggested in JWSR, and the collapse is excellent. Their mean values are
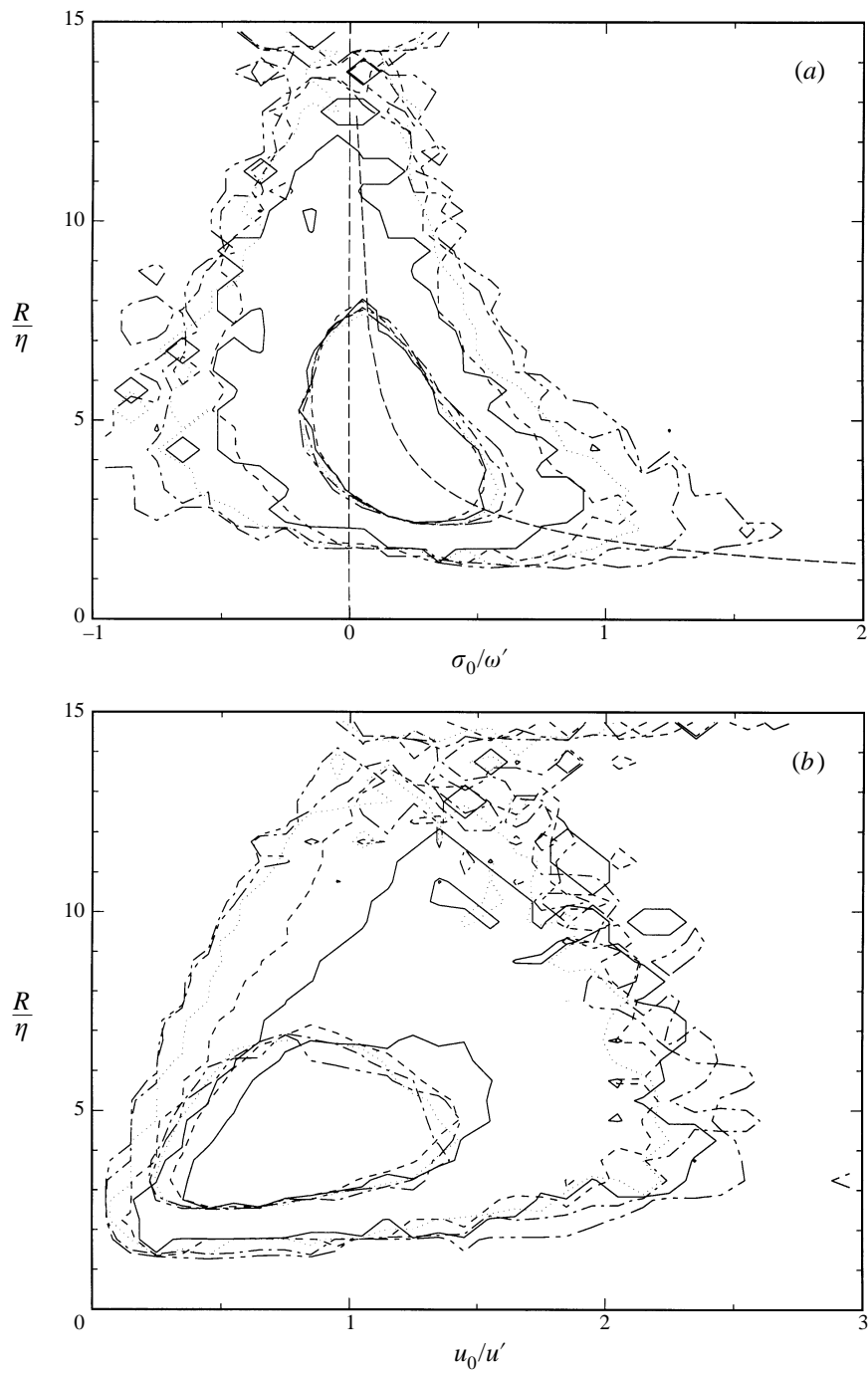
FIGURE 4. Joint p.d.f.s of properties of the filaments. (*a*) Axial stretching versus radius. (*b*) Maximum azimuthal velocity versus radius. Lines as in table 1. The dashed curve in (*a*) is the Burgers' radius. Two probability isolines are included for each case, $p_2 = 10^{-1}$ and $p_2 = 10^{-3}$.

summarized in table 1. In figure 3(b) we show, for those points at which $\sigma_0 > 0$, the p.d.f.s of the radii normalized with the Burgers' radius $R_b = 2(\nu/\sigma_0)^{1/2}$ of an equilibrium vortex stretched by the local σ_0. They collapse well and the maximum probability is at $R = R_b$, supporting the view that the filaments can be modelled as equilibrium Burgers' vortices (Jiménez 1992).

A different way of displaying the statistics is figure 4, which contains joint p.d.f.s of stretching and radius and of radius and azimuthal velocity. In each of them we have given two probability isolines for each Reynolds number, one corresponding to the central part of the p.d.f., and another to the outer tails. Figure 4(a) confirms that the p.d.f.s cluster around the local Burgers' radius, which is given as the dashed curve. As the Reynolds number increases, some of the filaments are subject to stronger stretching, and their radii are particularly close to the Burgers' limit. Note that the lower edge of the $p_2 = 10^{-3}$ isoline is in all cases very near the grid resolution $\Delta x/\eta = \pi/2$. There is little doubt that, were it not for this numerical limitation, these rightmost tails of the joint p.d.f.s would follow still more closely the Burgers' line, and this is confirmed by the $k_{max}\eta = 4$ simulations at the two lowest Reynolds numbers (not shown).

The mean stretching, which is mostly associated with points inside the $p_2 = 10^{-1}$ isolines in figure 4(a), scales with ω' independently of Re_λ, and there is a fairly large probability of finding points along the filaments at which the strain is compressive. It was shown by Jiménez & Wray (1994a, b) that the statistics of the stretching along the filament axes are essentially the same as in the bulk of the flow field. The filaments are not linked to locations where the stretching is particularly high, and the stretching that they feel is the background turbulent flow.

Figure 4(b) addresses the scaling of the azimuthal velocity with the large-scale velocity fluctuation u'. This is inconsistent with the Kolmogorov scaling, which requires that the velocity differences across lengths of $O(\eta)$ should be $O(u'Re_\lambda^{-1/2})$. The unconditional p.d.f.s in figure 3(d) leave the possibility that the large azimuthal velocities might be associated with points where the filaments are locally thick, but 4(b) shows that this is not the case. The azimuthal velocity is bounded above by approximately $2.5u'$, independently of Re_λ, and this limit is reached by the filaments with the narrowest radii.

Since, for a given circulation, the velocity difference across a stretched vortex increases with decreasing radius, it is not surprising that the thinner filaments contain the highest azimuthal velocities, but that the velocity across a dissipative length scale should be bounded by a large-scale quantity such as u' needs explanation. One was offered by Jiménez & Wray (1994a) and VJO who argued that there is a natural limit beyond which a Burgers' vortex of finite length cannot be stretched before it induces axial currents which counteract the applied strain. It turns out that this mechanism limits the maximum azimuthal velocity to be of the same order as the straining velocity differences applied along the vortex axes. Thus while vorticity can be amplified by stretching, velocity cannot and, if the maximum velocity difference available for stretching the filaments is $O(u')$, their maximum azimuthal velocity cannot increase beyond it. The argument also implies that filaments whose azimuthal velocity is $O(u')$ should be long enough that the velocity difference between their end-points is of that order, which usually requires lengths of the order of the integral scale. Lengths of that magnitude have been reported in all the observations of strong filaments, and are confirmed below.

The statistics discussed in the previous paragraphs should be interpreted with care
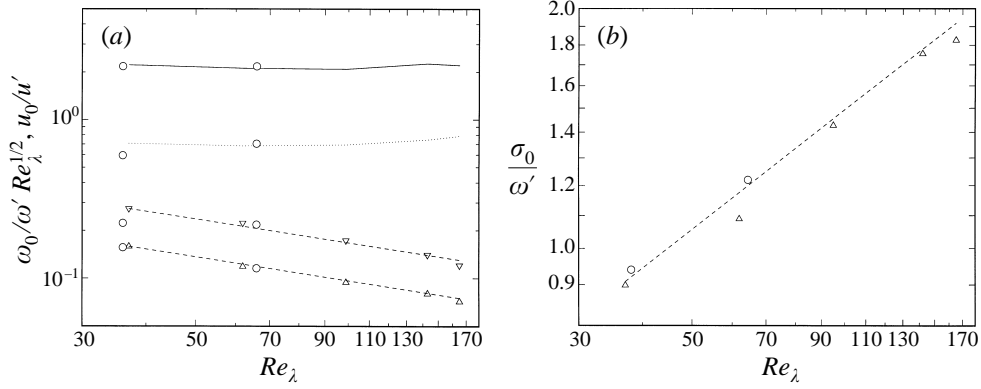
FIGURE 5. Minimum and maximum values of the filament properties at which their p.d.f.s intersect a fixed probability density level. (*a*) Vorticity at $p = 10^{-1}$: △, minimum; ········, maximum. Azimuthal velocity at $p = 10^{-2}$: ▽, minimum; ———, maximum. Dashed lines have slope $Re_\lambda^{-1/2}$. (*b*) Global maximum of the axial stretching along the detected filaments for the different Re_λ. The triangles are data for $k_{max}\eta = 2$. The dashed line has slope $Re_\lambda^{1/2}$. The open circles in both figures are data for $k_{max}\eta = 4$.

in view of the considerations discussed in §3 on the variable size of the samples. Since the tracking algorithm identifies first the strongest filaments, which include the most stretched segments with the narrowest radii and the strongest vorticities, only those extreme values should be trusted independently of the sample size, while mean velocities and radii may respectively be expected to decrease and increase if the sample is made much larger.

In figure 5(*a*) we give the minimum and maximum values of the axial vorticity and azimuthal velocity, measured at a fixed probability level. These are the two points at which each p.d.f. in figure 3 falls below a given probability. The maxima scale as $u_{max} \sim u'$ and $\omega_{max} \sim \omega' Re_\lambda^{1/2}$, as discussed above, but the minima do not. The two dashed lines in the figure are proportional to $Re_\lambda^{-1/2}$, and imply that $\omega_{min} \sim \omega'$ and $u_{min} \sim u' Re_\lambda^{-1/2}$. Those are the Kolmogorov scalings for features of size η, and represent the points at which the filaments merge into the background vorticity field. The fact that our analysis is able to identify the regular scalings of the weaker parts of the structures increases our confidence on the anomalous ones found for the stronger ones.

The minimum vortex radius has not been included in this analysis, since figure 4(*a*) implies that it may be contaminated by the size of the grid, and suggests that it is better to plot the maximum axial stretching as a function of Re_λ, and to assume that the minimum radius is proportional to the corresponding Burgers' limit. This is done in figure 5(*b*), with the result, to be discussed later, that

$$\sigma_{max} \sim \omega' Re_\lambda^{1/2}, \tag{4.1}$$

implying that

$$R_{min} \sim \eta Re_\lambda^{-1/4}. \tag{4.2}$$

Note that all these figures include data from the $k_{max}\eta = 4$ simulations, which are within the statistical uncertainty of the lower resolution ones.
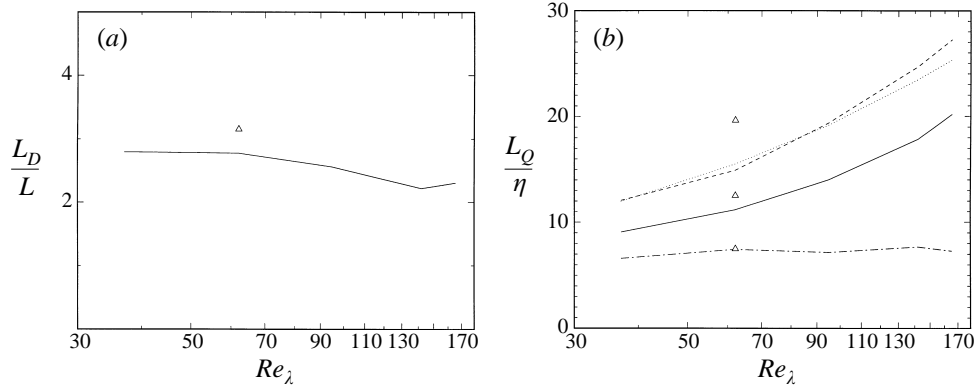
FIGURE 6. Filament lengths as a function of the Reynolds number. (*a*) Detected length. (*b*) Correlation lengths for various properties: ———— , radius; – – – – , axial vorticity; —·— , axial stretching. The dotted line in (*b*) is the Taylor microscale and the triangles in both cases are the decaying field.

4.2. *Filament length*

Another quantity of interest is the length of individual filaments. It is related to their lifetime because a filament can only become coherent over a length ℓ if its lifetime is at least ℓ/u_ℓ, where u_ℓ is its velocity scale. Visual observation of experiments by Douady, Couder & Brachet (1991) and numerical simulations by Vincent & Menneguzzi (1991) and JWSR suggest that the characteristic length is of the order of the integral length of the flow, but there has been little systematic study of its Reynolds number dependence. The implied lifetimes are of the order of the integral eddy-turnover time, in agreement with Douady *et al.* (1991), Villasenor & Vincent (1992) and Villermaux, Sixou & Gagne (1995).

The definition of the length depends on the observation procedure. Our vortex tracker abandons a filament either when it intersects a previously identified one or when its axial vorticity falls below ω'. The resulting average length is of the order of a few integral lengths, with a slightly decreasing trend as the Reynolds number increases (figure 6*a*). The probability distribution of filament lengths (not shown) is roughly exponential, with standard deviations of the order of 0.6–0.7 of the mean.

A more objective length can be defined in terms of the autocorrelation function of some filament property ξ, expressed in terms of the arc length s,

$$Q_\xi(s) = \langle \xi(s' + s)\xi(s')\rangle / \langle \xi^2(s')\rangle, \tag{4.3}$$

where ξ has been normalized so that $\langle \xi \rangle = 0$. The length is then defined as

$$L_Q = \int_0^{s_0} Q_\xi(s)\,\mathrm{d}s, \tag{4.4}$$

where s_0 is the point where the autocorrelation function first goes negative, and it is displayed in figure 6(*b*) for three different filament properties. It is clear that they separate in two groups. The length based on the axial stretching scales with the Kolmogorov scale, while those based on actual filament properties scale with the Taylor microscale $\eta Re_\lambda^{1/2}$.

The correlation length of the stretching is comparable to the diameter of the filaments, and to the Kolmogorov length. Since the latter is also the characteristic correlation length of the velocity gradients over the whole flow, this is consistent with the previous conclusion that the stretching felt by the filaments is the background

strain of the flow, and that they are natural consequences of this background. Note that the filaments in the decaying field tend to be somewhat longer than in the forced ones.

That the Taylor microscale should appear in this context is not surprising. Consider a vortex line of length $L \gg \lambda$ and define its unit tangent t and normal n, and a length element $\mathrm{d}\ell$. The line integral of the vorticity stretching due to the velocity gradient tensor, S, can be written as

$$\int_a^b t \cdot S \cdot t \, \mathrm{d}\ell = u \cdot t\big|_a^b - \int_a^b \rho^{-1} u \cdot n \, \mathrm{d}\ell, \qquad (4.5)$$

where ρ is the local radius of curvature and u is the flow velocity. We have seen that the mean value of the stretching is $O(\omega')$, so that the integral on the left of the equation is $O(\omega' L)$. It is known experimentally that the velocity probability distributions in turbulence are free from intermittency effects, in the sense that higher Re_λ do not correspond to wider velocity tails (Anselmet *et al.* 1984), so that the order of magnitude of the velocities in the right-hand side of (4.5) is at most u'. This implies that the radius of curvature of the line has to be $\rho = O(u'/\omega') = O(\lambda)$ for both sides of the equation to be of the same order, and that vortex lines have to be geometrically complex over distances much longer than λ.

4.3. *Filament volume*

Most of the strong vorticity in the flow field is in the form of filaments. This, which has been repeatedly reported from visual analyses of simulations (see references in §1), is confirmed by the present tracking data, and serves as an independent check of the thoroughness of the search.

Consider a short filament segment of length $\mathrm{d}\ell$. The volume filled by vorticity weaker than ω is $\mathrm{d}V = 2\pi r(\omega)\,\mathrm{d}r\,\mathrm{d}\ell$, and it follows from (3.1) that its contribution to the global probability distribution of the vorticity magnitude over a volume V_T is

$$\frac{1}{V_T}\frac{\mathrm{d}V}{\mathrm{d}\omega} = \frac{1}{V_T}\frac{\pi R^2}{\omega}\,\mathrm{d}\ell, \quad \text{if} \quad \omega \leqslant \omega_0. \qquad (4.6)$$

The contribution to the global p.d.f. from a set of filaments can then be expressed as a Lebesgue integral

$$\tilde{p}(\omega) = \frac{\pi}{V_T \omega} \int_{\omega_0 \geqslant \omega} R^2\,\mathrm{d}\ell(\omega_0), \qquad (4.7)$$

which can be computed from the filament sample and compared to the p.d.f.s obtained from the whole flow. Figure 7(*a*) presents the global p.d.f.s, with their characteristic Reynolds-number-dependent intermittent tails. In figure 7(*b*), they are compared at two Reynolds numbers to the contribution (4.7) from the detected filaments. The tails coincide in both cases, showing that essentially all the strong vorticity has been captured in the form of filaments. There are no adjustable parameters in this fit, which holds for all the other simulations.

The abscissae in figure 7(*b*) have been normalized with the vorticity scale of the filaments, $\omega_f = \omega' Re_\lambda^{1/2}$, and it is interesting that, even if the tails of the probability distributions have different slopes when they are normalized with ω', as in figure 7(*a*), they are more or less parallel to each other in figure 7(*b*). They can be collapsed using the new normalization if, in addition, each p.d.f. is divided by the empirical volume fraction $V(Re_\lambda) = p(\omega/\omega_f > 0.5)$. The p.d.f. can then be written as

$$p(\omega) = \omega_f^{-1} V(Re_\lambda)\,p_0(\omega/\omega_f), \qquad (4.8)$$
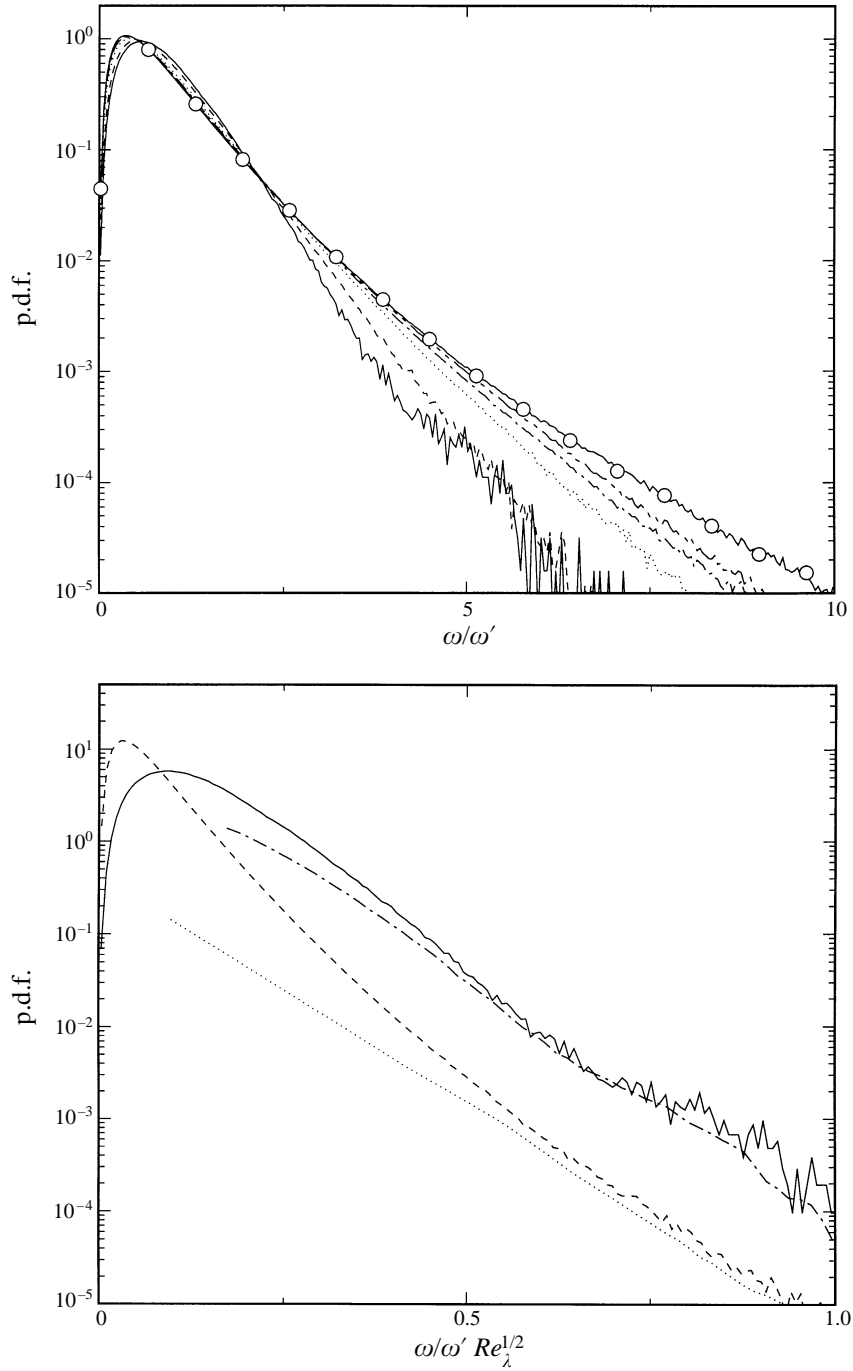
FIGURE 7. Probability density functions for the vorticity magnitude over the whole flow. (*a*) Calculated directly from the simulations in table 1. Lines as in table 1. (*b*) Tails of the p.d.f. for $\omega > \omega'$, computed from the filament statistics, compared to the actual distributions. $Re_\lambda = 37$: ———, from simulation; —·—, from filaments. $Re_\lambda = 142$: - - - -, from simulation; ········, from filaments.
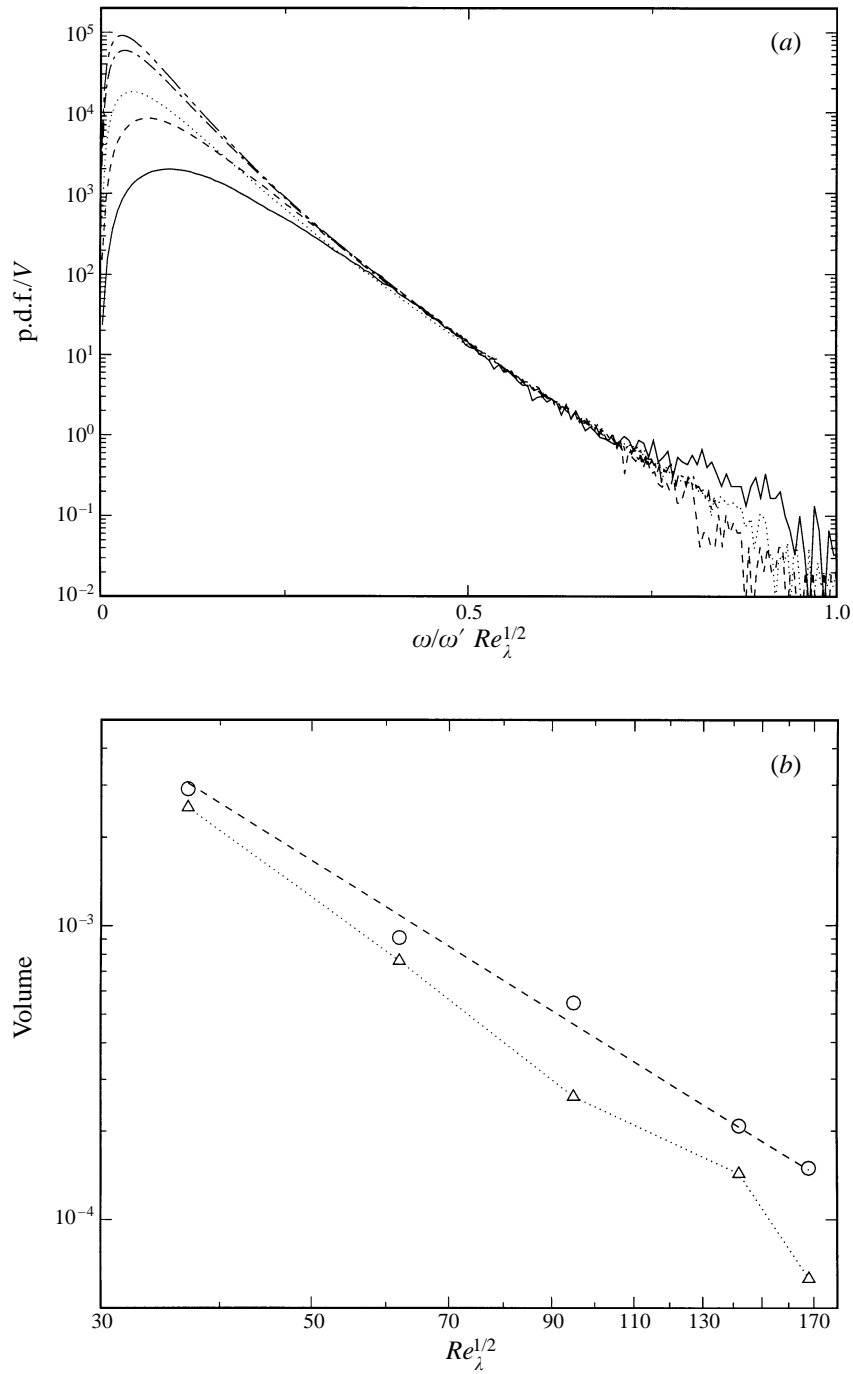
FIGURE 8. (*a*) P.d.f. of the vorticity magnitude over the whole field, normalized as in (4.8). (*b*) Volume fraction for $\omega > 0.5\omega_f$ as a function of Reynolds number. $\circ$, from global p.d.f.s; $\triangle$, from filament contribution (4.7); $----$, $4.16Re_\lambda^{-2}$. The dotted line joining the triangles is drawn to aid the eye.

where p_0 is universal in the tail region. The collapse is shown in figure 8(a), and the volume fractions are given as open circles in figure 8(b). They vary as Re_λ^{-2}, as already found by Jiménez & Wray (1994b) from filament data. Contrary to the stretched exponential behaviour of the tails of the p.d.f.s of the longitudinal velocity gradients (Kailasnath, Sreenivasan & Stolovitzky 1992; Tabeling *et al.* 1996), the tails of our vorticity p.d.f.s are well represented, beyond $\omega/\omega_f \approx 0.3$, by

$$p_0(\xi) \approx 1.93 \times 10^4 \exp(-14.4\,\xi). \tag{4.9}$$

Note that there is no contradiction in that the p.d.f. of the vorticity behaves differently from those of the velocity gradients. Most of the contribution of a vortex to the statistics of the gradients comes from points outside its core, where the gradients are still large but where the vorticity is already zero. It is actually possible to form realistic statistics for the gradients using vortices with uniform cores, for which the vorticity p.d.f. would be two delta functions. This is true both for the longitudinal and for the transverse gradients, as was shown in a two-dimensional example by Jiménez (1996).

What fraction of the filaments is detected by the tracker can be estimated by comparing $V(Re_\lambda)$ with the volumes obtained by integrating the filament contribution (4.7). The latter are given in the figure as open triangles, and decline somewhat faster with Re_λ, reflecting the difficulty of processing the larger files. The effect on the averages should be moderate. It follows from (4.9) that the difference in volume fractions detected by the tracker at the highest and lowest Reynolds numbers correspond to a vorticity difference of approximately $0.05\omega_f$.

If we use the scaling of the vortex radii as η, which is proportional to $L_\epsilon Re_\lambda^{-3/2}$, and combine it with the estimate of their volume fraction as Re_λ^{-2} we obtain that the total length of the filaments contained in a fluid volume of the order of the cube of the integral length increases as Re_λ. This is confirmed by the relatively good collapse of the different curves in figure 2, which are scaled in that way, and means that the filaments become more prevalent at high Reynolds numbers, even if their volume shrinks because they become thinner. The best fit to figure 2 is that the total length per unit volume of filaments which contain somewhere an axial vorticity larger than $\omega_{0,max}$ is

$$L \sim L_\epsilon^{-2} Re_\lambda \exp(-8\,\omega_{0,max}/\omega_f). \tag{4.10}$$

5. Discussion

We have shown that, at the Reynolds numbers of our simulations, the strong coherent vortices identified by our tracker have radii which scale as the Kolmogorov length, and azimuthal velocities which are of the order of the large-scale velocity fluctuations in the flow u'. The average axial stretching, σ, scales like ω'. These scalings confirm those found by JWSR and by the later simulations and laboratory experiments cited in the introduction.

Since the Kolmogorov scale $\eta = (\nu/\omega')^{1/2}$ is proportional to the Burgers' viscous length for strains of $O(\omega')$, the scalings of σ and R are consistent with a simple model in which the filaments are created as Burgers' dissipative structures by a turbulent background in which, according to the classical Kolmogorov picture of the flow, the velocity gradients are proportional to ω'.

Cadot *et al.* (1995) also find coherent vortices whose internal velocities scale with u', and whose lengths are $O(L_\epsilon)$, in agreement with our tracking results. Their experiments

cannot determine the radii directly, but the authors suggest, on the basis of theoretical arguments and of incomplete measurements, that they should be of the order of the Taylor microscale λ. Their argument is that λ is the Burger's limit for the large-scale strain u'/L_ϵ, which is the only possible coherent strain over the observed lengths. They also predict that there should be a range of smaller filaments, each of them driven by the strongest possible coherent strain over their lengths, whose most intense members would have both radii and lengths of $O(\eta)$.

Our observations disagree with the last conclusion. We find vortices whose radius is $O(\eta)$, but whose length is $O(L_\epsilon)$. Even if within them we find a shorter axial correlation length for the radius and for the vorticity which is $O(\lambda)$, it is still longer than the Kolmogorov scale. Moreover, our observations disagree with a key assumption of Cadot *et al.* (1995), which is that the axial stretching must be coherent along the length of the vortex. We find correlation lengths for the stretching which are shorter, $O(\eta)$, than the vortex length, comparable to the scale of the velocity gradients over the bulk of the flow. Such stretching would be felt by the vortices as spatially uncorrelated. Moreover, since the filaments sweep through these small structures in times comparable to their own rotation times, they would also see the stretching as effectively uncorrelated in time.

It was demonstrated in VJO and Verzicco & Jiménez (1997) that the axial length scales of the stretching strain and of the vortex properties are decoupled in inhomogeneous vortices by axial Kelvin waves driven by the variable pressure along their axes. They showed that effectively infinitely-long vortices can be maintained by axially inhomogeneous, locally compressive, strains, even in the limiting case in which the mean stretching is zero. The resulting radii are of the order of the Burgers' radius corresponding to the r.m.s. of the stretching, rather than to its mean. We have shown above that the axial strain along the filaments is compressive along a substantial percentage of its length but that, where it is extensive, the vortex radii scale as in Burgers' vortices. Axial modulations of the vorticity of the filaments, resembling waves, were observed by Villasenor & Vincent (1992). The decoupling between the axial scales of the vortices and that of the stretching provides a mechanism by which long vortices can be maintained with diameters of order η, which is the Burgers' limit for the r.m.s. strain of $O(\omega')$. It also suggests that we are not observing the vortices at their time of formation, but only after they have become strong enough to decouple from the background.

Another important consequence of the argument in VJO is that the azimuthal velocity of a vortex produced by an inhomogeneous stretching is not limited by the magnitude of the stretching, but by the maximum velocity difference along its axis. If a vortex is subject to a local stretching which would drive it to a radius which is too thin, or to an azimuthal velocity which is too high, it bursts instead of pinching. Thus if the maximum large-scale velocity difference in the flow is $O(u')$, no vortex can be strained beyond the stage at which its azimuthal velocity becomes of that order. This is consistent with the velocity scaling mentioned above, and with the lack of any Reynolds number trend in the high end of the azimuthal velocity p.d.f.s in figures 3(*d*) and 4(*b*).

Scalings different from the ones discussed here have been proposed on theoretical grounds by other investigators. It has already been noted in JWSR that the dependence of the mean value of ω_0/ω' on the Reynolds number could be consistent, over the range of our simulations, with powers different from $Re_\lambda^{1/2}$. Rasmussen (1995) noted that they could actually be better fitted by $Re_\lambda^{1/3}$, and proposed a model to explain

that dependence which is based on a helicity cascade. It is clear from a consideration of the bounds in figure 5(a) and from inspection of figure 3(c), that most of the deviations of the mean vorticity from the $Re_\lambda^{1/2}$ scaling are due to the cutoff of the p.d.f.s below ω', and that the 'intense' parts of the distributions scale better than the means. Over the range of Reynolds numbers of the present simulations, the difference between $Re_\lambda^{1/3}$ and $Re_\lambda^{1/2}$ would amount to a decrease of $\omega_0/\omega' Re_\lambda^{1/2}$ by a factor of 1.3, which is only barely consistent with the slight increase observed, for example, in the maximum values in figure 5(a). Moreover, as mentioned in the introduction, the scalings laws $R \sim \eta$ and $u_0 \sim u'$ have recently been extended experimentally to $Re_\lambda \approx 800$, and they imply a $Re_\lambda^{1/2}$ scaling for the vorticity. The drift of $Re_\lambda^{1/3}$ over that range would be a factor of 1.7, which is inconsistent with the data. There is, however, nothing in our data to preclude this, or other, cascading mechanism from being responsible for vortices weaker than the ones studied here.

5.1. *The coherent cascade*

Although the most probable axial strain felt by the filaments is $O(\omega')$, independently of Re_λ, it was shown in figure 5(b) that its maximum value increases with Reynolds number as $\omega' Re_\lambda^{1/2}$. This is of the order of the axial vorticity and, if it is interpreted as evidence of self-stretching, it would imply that the radius of curvature of a self-stretching vortex is of the order of its core radius, which is the correct scaling for the instabilities of high Reynolds number vortex cores under triaxial strains (Saffman 1992). Another interpretation would be that the high stretchings are due to interactions between filaments, but it is shown in the Appendix that the probability of intersection is too low to account for the observations.

It follows from the previous scalings that the internal Reynolds number of the observed vortices is $\gamma/\nu \approx 20 Re_\lambda^{1/2}$, and it has already been observed in JWSR that it is unlikely that they would remain stable for high Re_λ. The previous observation suggests that they do not, and that the highest observed strains are due to the initial stages of their instability. That these high strains are only found in the extreme tails of the distributions suggests that the unstable regions are confined to a small fraction of the total length, presumably due to the weak magnitude of the background perturbations compared to the vorticity of the filaments.

Assuming that the radii, R_2, of the self-stretched segments scale like the Burgers' limit corresponding to the stretching that they feel, $O(\omega' Re_\lambda^{1/2})$, and that their azimuthal velocities are bounded, as before, by their driving velocity, $\omega_1 \eta \sim u'$, it follows that

$$R_2 \sim \eta Re_\lambda^{-1/4}, \qquad \gamma_2/\nu \sim Re_\lambda^{1/4}. \tag{5.1}$$

These pinched segments have lengths which are of the order of the radius of the parent vortex, $\ell_2 \sim R_1 \sim \eta$, which is the scale over which the instability develops. For large Re_λ such a vortex segment is still elongated and its internal Reynolds number is still high. It would again become unstable along sections with lengths of the order of its own radius, along which the self-stretching would be $\sigma_3 \sim u'/R_2 \sim \omega' Re^{3/4}$, and the radius would be thinner. This leads to a hierarchy of self-stretching instabilities in which two consecutive levels are related by

$$\sigma_n \sim u'/R_{n-1}, \qquad R_n \sim (\nu/\sigma_n)^{1/2} \sim (\nu R_{n-1}/u')^{1/2}, \qquad \ell_n \sim R_{n-1}, \tag{5.2}$$

and which asymptotes to

$$R_\infty \sim \eta_0 = \nu/u' \sim \eta Re_\lambda^{-1/2}, \tag{5.3}$$

$$\sigma_\infty \sim u'^2/v \sim \omega' Re_\lambda, \tag{5.4}$$

$$\gamma_\infty/v \sim 1. \tag{5.5}$$

$$\ell_\infty = R_\infty \sim \eta_0. \tag{5.6}$$

This defines an absolute inner limit, η_0, for the radii of the intermittent structures which is below the Kolmogorov scale, and which is reached on small subsets of the flow through a coherent cascade of instabilities, instead of through the classical space-filling Kolmogorov mechanism.

Note that, because $\Delta u \sim \gamma/R$ and the circulation is conserved during stretching, a vortex for which $\Delta u = O(u')$ cannot pinch as a single unit. It has to break into several braids, each of which carries part of the original circulation. This braiding process has been observed by Cadot *et al.* (1995), and a possible mechanism is suggested by the structure of strong vortices subject to inhomogeneous straining in VJO (see figures 11–14 in that paper). When a vortex is strained beyond the limit at which its azimuthal velocity would become larger than the driving axial velocity difference, it becomes hollow and the vorticity is expelled into a cylindrical sheet whose thickness is the Burgers' length of the driving strain. This sheet is unstable to Kelvin–Helmholtz waves and should break into longitudinal vortices, each of which would have the correct radius and circulation for (5.2).

That the cascade could occasionally extend beyond the Kolmogorov scale has already been noted by Paladin & Vulpiani (1987) and later by Frisch & Vergassola (1991), in the context of the multifractal model of turbulence (Parisi & Frisch 1985). The latter describes turbulence as a collection of interpenetrating components, on each of which the velocity difference over a distance R behaves as

$$\Delta u(R)/u' \sim (R/L_\epsilon)^\alpha \quad \text{as} \quad R \to 0. \tag{5.7}$$

The successive vortex instabilities of the coherent cascade described in (5.2)–(5.6) define a component in which the velocity difference does not change as the scale shrinks, and whose singularity exponent is therefore $\alpha = 0$. The set is defined at each length scale by the union of all the vortex segments which become unstable and pinch to the next level of (5.2). If we define the end of any α-component as the scale η_α at which the Reynolds number $R\Delta u/v$ reaches unity, we obtain

$$\eta_\alpha = \left(v L_\epsilon^\alpha/u'\right)^{1/(\alpha+1)}. \tag{5.8}$$

The classical Kolmogorov scale, $\eta_{1/3}$, corresponds to the space-filling energy cascade for which $\alpha = 1/3$, while (5.3) corresponds to $\alpha = 0$.

There is no reason for the cascading process to start with filaments of the order of the Kolmogorov scale. Any object with a vorticity higher than the background would tend to become coherent, and should generically evolve into a cylindrical vortex, not necessarily slender, which is one of the few known stable solutions of the Euler equations (Vincent & Meneguzzi 1994). The axial waves described above would then connect these precursors into longer filaments (see figure 4 in VJO), as has been observed by Villasenor & Vincent (1992) and suggested by JWSR on theoretical grounds.

It is interesting that the largest coherent structures that can form in this way are vortices with $\Delta u \sim u'$ and vorticities just above ω', which would therefore have radii of order $R_0 \sim u'/\omega' \sim \lambda$. They may correspond to the $O(\lambda)$ vortices observed by Cadot *et al.* (1995). If we take them to be the initial structures in the hierarchy (5.2), the next radius would be $R_1 \sim \eta$, and the precursors of the filaments described in
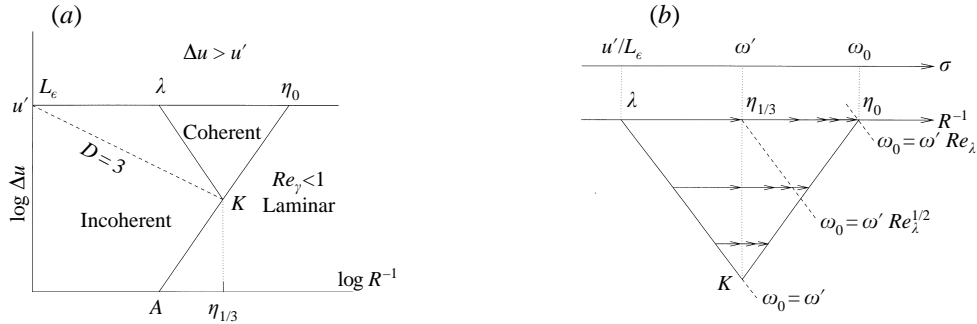
FIGURE 9. Schematic representation of the types of turbulent structures in terms of the velocity differences that they contain and of their transverse length scale. (*a*) Only structures within the triangle $\lambda\eta_0 K$, for which the characteristic vorticity is larger than ω' and the Reynolds number is large enough, can be expected to be coherent. This region is enlarged in (*b*).

this paper would correspond to secondary instabilities of primary $O(\lambda)$ structures, as originally proposed by Saffman (1968). This would be consistent with the observation that the filaments with $R = O(\eta)$ have an internal axial length scale of $O(\lambda)$, and is essentially a qualitative restatement of the argument in (4.5).

Note that the process described up to now gives only an upper bound for the intensity of the coherent vortices, as limited by the requirement that the azimuthal velocity should not exceed $O(u')$. There is no need for a vortex to have velocities of that order to survive, and we can imagine vortices that first become coherent with $\omega \approx \omega'$ but with $\Delta u < u'$. Their initial radii would be $\Delta u/\omega'$. If their internal Reynolds numbers are large, they would cascade through a sequence of instabilities as in (5.2)–(5.6), but with Δu substituted for u'. It is easy to see that the first stage of the cascade always generates vortices with $R \sim \eta$, and that these weaker hierarchies accumulate to vortices of unit elongation and Reynolds number whose radius is $R_\infty(\Delta u) = v/\Delta u \geqslant \eta_0$. The cascade described above is just the strongest of this family of cascades, and it is therefore the most easily observed, but all of them generate filaments with peak vorticities in the range $\omega' \leqslant \omega_0 \leqslant \omega' Re_\lambda^{1/2}$, and contribute to the anomalous tails of the vorticity distributions. There is in principle the possibility of a certain amount of exchange between different members of the family, such as when a high-velocity vortex interacts with a low-velocity one and strains it into a higher-velocity class. We have seen that such interactions are rare, at least once the vortices reach $R \sim O(\eta)$. Vice versa, an imperfect braiding might convert part of a high-velocity vortex to a lower velocity. A more widespread mechanism is probably the vortex connection process mentioned above in which short precursors are collected into longer filaments. In that process fluid is entrained into the end points of an existing vortex segment by the low pressure in its core, and the ambient vorticity is organized into a coherent bundle. The result is the promotion of incoherent fluid to a high Δu-class. Otherwise each cascade is limited by the VJO straining argument to the maximum velocity difference with which it starts its coherent life.

Structures can then be classified in terms of the Δu–R diagram in figure 9(*a*). To the right of the line $AK\eta_0$ the Reynolds number is small and viscous dissipation dominates. Turbulence exists only to the left of that line. To the left of λK the vorticity of the structures $\Delta u/R$ is lower than the r.m.s. vorticity ω', and no coherence is possible. The line $L_\epsilon K$ is in this turbulent region and represents the space-filling Kolmogorov energy cascade $\Delta u \sim R^{1/3}$. Point K is the classical Kolmogorov scale.
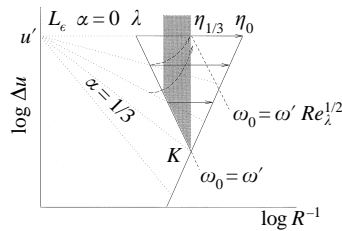
FIGURE 10. Sketch of the velocity–length classification of the turbulent structures, showing the α-components of the multifractal model as dotted lines, and the coherent cascades as solid arrows. The dashed arrows represent the fluid capture mechanism by which strong vortices grow axially, as discussed in the text. The shaded region is the one accessible to our vortex tracker, and corresponds roughly to figure 4(*b*).

Coherent structures exist in the triangle $\lambda\eta_0 K$, which would be the seat of intermittency and which is enlarged in figure 9(*b*). Radii in this sketch decrease from left to right, while the driving strains do the opposite. The oblique dashed lines represent constant core vorticities, which increase towards the top right corner. The paths of three typical coherent vortices during the cascade are represented by arrows. They are created at the $\omega_0 = \omega'$ line and migrate horizontally towards increasing vorticity with constant velocity increments, until they reach the viscous limit along the line $\eta_0 K$.

There is a difficulty with the previous arguments. The cascade in (5.2) assumes that viscosity is the only diffusion process limiting the radius of the vortices, which is only true for laminar flow, while we are proposing that the structures are internally turbulent at least over part of their length. A possible explanation is that vortices form as turbulent structures, which would have larger radii, but that their cores eventually laminarize under the effect of their own rotation. It is known that rotation inhibits energy transfer in homogeneous turbulence (Cambon & Jacquin 1989), and Zeman (1994) has shown that the effect should be active whenever the imposed rotation is comparable with or higher than the inverse eddy-turnover time of the turbulent scales. For the strong vortices that concern us here, whose vorticity is at least $O(\omega')$, that would be true for all the scales. Relaminarization by strong vorticity is a well-known effect in the trailing vortices of aircraft, whose Reynolds numbers are much higher than those involved here (Bandyopadhyay, Stead & Ash 1991; Zeman 1985), and Andreotti *et al.* (1997) have observed a large decrease in the turbulent intensity in the core of a stationary vortex within a turbulent flow. The observed filaments would then be those that have persisted for times long enough to develop laminar cores.

5.2. *Multifractal versus coherent cascades*

We are now in a position to compare the coherent Δu-cascades described in the previous section with the classical description of intermittency in the multifractal model. Consider the sketch in figure 10, which is a version of the one in figure 9. The multifractal α-sets (5.7) lie along the dotted lines radiating from L_ϵ, with each slope corresponding to a different value of α. These sets are kinematic, and there is no implication of causality among their points. The multifractal model starts from the observation that there are no preferred length or velocity scales within the inertial range, and deduces from it that each α-set is a self-similar fractal (Parisi & Frisch 1985). The volume of a set is then proportional to R^{3-D}, where $D(\alpha)$ is interpreted as a fractal dimension. The multifractal spectrum, which relates $D(\alpha)$ to the singularity

exponent, has been measured in the inertial range for several flows and is summarized by Sreenivasan (1991).

In the multifractal model, each α-set reaches the viscous line $K\eta_0$ at its local Kolmogorov scale (5.8). In our model of coherent cascades, all the α-sets for which $\alpha \leqslant 1/3$ reach first the line $K\lambda$ where $\omega \approx \omega'$. They then become organized into filaments and cascade at constant Δu towards the viscous limit. These coherent cascades are represented in the figure as horizontal solid arrows, which imply causality. The only cascade which is also an α-set is $\Delta u \approx u'$, for which $\alpha = 0$.

We have seen that the coherent vortices are viscous objects, even if their Reynolds numbers are large. This, together with the constant internal velocity of each cascade, defines time and length scales, and invalidates the self-similarity assumption of the multifractal model. The overall picture is then an incoherent inertial range to the left of λK, which should be well-described by the multifractal model, and a coherent region to its right, where the multifractal scaling does not apply. Both regions are bounded on the right by the dissipative limit. A structure first cascades incoherently through the inertial range, not necessarily along an α-set, and eventually, if it reaches $\omega_0 \approx \omega'$ while its Reynolds number is still high, cascades as a filament along one of the coherent lines. Since the Kolmogorov energy dissipation argument guarantees that most points are concentrated on the $\alpha = 1/3$ set, the previous model predicts that the intermittent sets are relatively sparse, in qualitative agreement with our observations in §4.3 of the total volume occupied by the coherent vortices. We will see below that this simple picture has to be modified slightly to account quantitatively for those observations.

The shaded area in figure 10 contains the structures studied in this paper, and corresponds to the roughly triangular region in figure 4(b), although in a different orientation.

The two vertical borders of this region, which would be horizontal in figure 4(b), represent limitations of our tracker and of the resolution of the simulations, and the diagonal along λK, which corresponds to the diagonal limit in the p.d.f.s in figure 4(b), is also to a certain extent artificial, since the tracker rejects filaments whose maximum vorticity is below ω'.

It is then clear that the statistics in figures 3 and 4 are biased towards intense, narrow filaments, and that the scalings have been chosen so as to collapse the parts of the p.d.f.s which represent narrow radii, high velocities and intense vorticities, roughly corresponding to the neighbourhood of the point labelled as $\eta_{1/3}$ in figure 10. The limitations of our technique and of our simulations make it difficult to draw conclusions on the statistical distribution of structures over the rest of the coherence triangle $\lambda\eta_0 K$.

This reflects our inability to study inertial length scales. Although our simulations contain a short range of approximately $k^{-5/3}$ energy spectrum, none of them has an inertial range in the classical sense that the Kolmogorov 4/5 law is satisfied (Jiménez 1997), and the problem can only be overcome by going to higher Reynolds numbers. An examination of the experimental spectra and structure functions available in the literature suggests that a well-developed inertial range requires at least $Re_\lambda \approx 600$ (Anselmet *et al.* 1984; Saddoughi & Veeravali 1994). The requirements to study the coherent region might actually be stricter, since it only takes the last third of the inertial range. To study the properties of possible sub-Kolmogorov coherent structures would require high Reynolds numbers and substantially better resolutions than the ones used here.
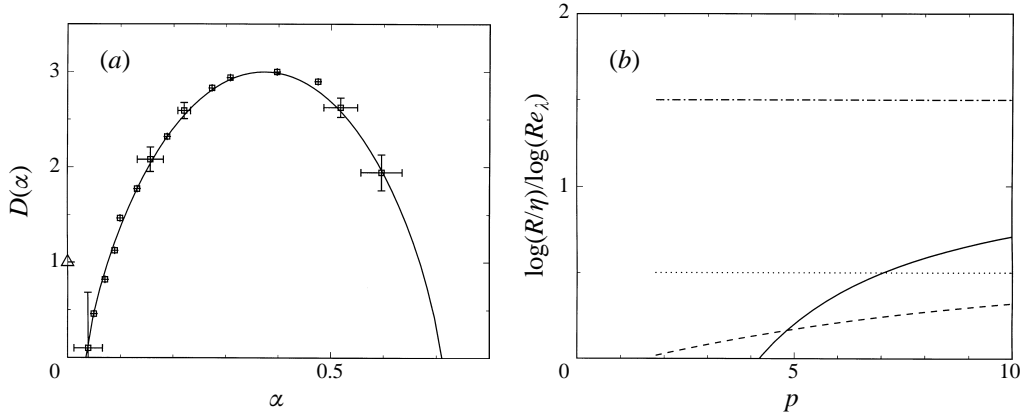
FIGURE 11. (a) Multifractal spectrum in the inertial range. □ , Experimental values from Sreenivasan (1991). △ , Coherent cascade, as discussed in the text. The solid line is a best fit to the experimental values from a simple multiplicative model (Jiménez 1997), to guide the eye. (b) Limiting length scales for self-similar multifractal scaling, as a function of the order of the structure function: ——— , due to the effect of the $O(\eta)$ filaments (5.17); – – – – , due to the weakest coherent structures (5.15); ········ , Taylor microscale; —·— , integral scale.

5.3. *Fractal dimensions*

In spite of the difficulties mentioned in the previous subsection, it is tempting to relate quantitatively our volume fraction data with the predictions of the multifractal model. As discussed above, this can only be done for the multifractal component $\alpha = 0$. The multifractal spectrum from Sreenivasan (1991) is reproduced in figure 11(a), and gives

$$D(0) \approx 0, \qquad (5.9)$$

which implies that the volume of the $\alpha = 0$ component decreases as R^3.

Obtaining fractal dimensions from our data implies estimating the total volume of the vortices in the cascade as a function of their radii. This can be done in two ways. Most simply we can read it directly from figure 8(b), which shows that the volume fraction on which $\omega > 0.5\omega_f$ is approximately $4Re_\lambda^{-2}$. This, together with the good collapse of the tails of the p.d.f.s in figure 3(d), implies that the volume containing velocity increments of $O(u')$ across distances of $O(\eta)$ varies in the same way.

This is inconsistent with a straight multifractal interpretation, in which the volume filled by those regions should vary as

$$V(\eta) \sim (\eta/L_\epsilon)^{3-D} \sim Re_\lambda^{-3(3-D)/2} \sim Re_\lambda^{-9/2}. \qquad (5.10)$$

The experimental variation, $V \sim Re_\lambda^{-2}$, would imply $D(0) \approx 5/3$, which is far from the values in figure 11(a). A different interpretation, more in agreement with our model, is that the multifractal component $\alpha = 0$ acts a source of velocity increments for the $\Delta u \approx u'$ coherent cascade. This happens at the point λ in figure 10, from where we may assume as a first approximation that a fixed fraction of the volume eventually decays into u' vortices at $R \approx \eta$. In this view the volume of the $\Delta u \approx u'$ vortices is fixed by the multifractal model at $R \approx \lambda$, and should scale as

$$V(\lambda) \sim (\lambda/L_\epsilon)^{3-D} \sim Re_\lambda^{D-3} \sim Re_\lambda^{-3}. \qquad (5.11)$$

This is larger than (5.10), but still smaller than the observed variation Re_λ^{-2}, which

would now imply $D(0) \approx 1$. This point is represented in figure 11(a), and is also far from the multifractal spectrum.

We have assumed above that a fixed fraction of the volume of the structures at the origin of a coherent cascade eventually decays along it. We will see in the next paragraph that that assumption is inconsistent with the limited data that can be derived from the present observations. It is however the decay model giving the lowest possible fractal dimension for the $\alpha = 0$ component, and therefore the one less at variance with the multifractal data. Consider any other scenario in which a smaller percentage of the structures at the point λ decays into coherent vortices with $R \approx \eta$. Since we know that the volume of the latter vary as Re_λ^{-2}, that of the former would have to vary slower with Re_λ, implying an even higher fractal dimension.

We can actually estimate the volume ratio across the first step of the coherent cascade, which carries vortices with radii $O(\lambda)$ to $R \sim O(\eta)$. The characteristic vorticities of the former are $O(\omega')$, while those of the latter are $O(\omega_f)$. We have seen in (4.10) that the total length of the coherent vortices whose vorticity is $O(\omega)$ decreases as $\exp(-8\omega/\omega_f)$. It is then easy to see that the *length* ratio between η- and λ-vortices is independent of Re_λ, essentially as the ratio between $\exp(-8)$ and $\exp(-8/Re_\lambda^{1/2}) \approx 1$. Their volumes are then related as the square of their radii,

$$V_1/V_0 \sim (\eta/\lambda)^2 \sim Re_\lambda. \tag{5.12}$$

This implies that $V_0 = V(\lambda) \sim Re_\lambda^{-1}$, and a multifractal dimension $D(0) \approx 2$.

The conclusion from this analysis is that there is more volume in the coherent η-vortices than can be explained on the basis of the multifractal spectrum and of the simple coherent cascades postulated in figure 10. Most of the volume present in the vortices has to come from processes which do not imply an initial velocity difference of $O(u')$. The likeliest candidate is the coalescence of short vortex segments into longer ones, discussed in §5.1, in which an intense short vortex grows along its axis by drawing new vortical fluid to its low-pressure core. This would modify figures 9–10 by providing an upwards drift of the coherent cascades towards the stronger ones, which has been included as dashed arrows in figure 10.

5.4. *Observables*

The description of the flow that has been developed in the previous subsections is based on the characteristics of the limited region of the coherence triangle that is accessible to our tracker. The existence of structures beyond that neighbourhood can only be inferred indirectly from the present data although, during the refereeing process of this paper, there have been two reports of organized filament-like structures with radii in the inertial range (Hosokawa, Oide & Yamamoto 1997; Porter, Woodward & Pouquet 1998). It is interesting to examine which would be their testable experimental consequences. At the moment, the most promising avenue seems to be laboratory experiments, since it seems unlikely that either the Reynolds number or the resolution of the numerical simulations will increase enough in the next few years to permit scaling studies in the inertial range. The purpose of this subsection is to collect in a single place a series of tests for different aspects of our model, in the hope that experimentalists will be motivated to undertake them.

(a) Several of the quantitative observations described in this paper can be checked experimentally. We have mentioned in the introduction that the existence of $\Delta u \sim u'$ structures at scales of the order of η has been confirmed experimentally up to $Re_\lambda \approx 800$. The results in §4.3 give information on the frequency of those structures which, to our knowledge, has still not been checked. The prediction is that the

probability of finding $\Delta u \geqslant u'/2$ over separations of order 4η, should vary as $4Re_\lambda^{-2}$. The same should be true for other $O(1)$ multiples of both quantities. We have published in Jiménez (1997) a compilation of existing p.d.f.s of velocity derivatives which supports this behaviour, but the result is not fully convincing because the limits of the available p.d.f.s were scaled with ω' rather than with ω_f, and because the resolution of the experiments was not uniform in η. Belin *et al.* (1997) have recently published a compilation of their own data, and favour a power of $Re_\lambda^{-3/2}$ in the range $Re_\lambda = 157$–700. Our own replotting of their data, which were kindly made available to us, appears to us to support our scaling, and the issue hinges on where to fit tails which are not exactly parallel. Also, the quality of the statistics in the tails of their p.d.f.s is not uniform with Re_λ, and neither is their probe resolution. A new careful experiment, or even a new uniform analysis of both data sets together with other data in the literature, should clarify the discrepancy.

(*b*) The test of probability scaling can be extended to the next step of the coherent cascade. In can be shown from the analysis of the p.d.f.s of the axial stretching that in that step, in which vortices of radius $R \sim \eta$ are pinched to $R \sim \eta Re_\lambda^{-1/4}$, the length ratio is also approximately independent of Re_λ. A representative value is

$$L_2/L_1 \approx 0.015 \quad \text{for} \quad \sigma_0/\omega_f \geqslant 0.05, \tag{5.13}$$

which, together with the previous result, implies that the probability of finding $O(u')$ velocity differences across distances of about $10\eta Re_\lambda^{-1/4}$, which is the Burgers' limit for the strain in (5.13), should be proportional to $Re_\lambda^{-5/2}$. Note that, because of the numerical factors, these length scales are not significantly shorter than η for most reasonable Reynolds numbers.

(*c*) Another set of results concerns the structure functions in the range of scales within the inertial range, but below $R \approx \lambda$. We have seen before that the existence of strong velocity structures beyond the Kolmogorov scale is predicted by the multifractal model, as well as by ours, and it is known that this 'multiscaling' implies a Reynolds number dependence of the structure functions at small separations (Frisch & Vergassola 1991; Passot *et al.* 1995). The difference between the two models is that, while the Reynolds number dependence should manifest itself below a fixed multiple of η in the multifractal case, the threshold would depend on Re_λ in ours. Consider $S_p = \langle \Delta u^p \rangle$. It is known from multifractal theory that, for scales in which (5.7) holds, each structure function is dominated by the α-set for which $p = \mathrm{d}D/\mathrm{d}\alpha$ (Frisch 1995, p. 145). This set intersects the $\omega \sim \omega'$ line at

$$\frac{\Delta u}{R} \sim \left(\frac{R}{L_\epsilon}\right)^{\alpha-1} \frac{u'}{L_\epsilon} \sim \omega', \tag{5.14}$$

$$R_p \sim \eta Re_\lambda^{3/2-1/(1-\alpha)}. \tag{5.15}$$

Below this separation the structure function should not be expected to behave self-similarly as a power of R. It tends to $R_p \sim \eta$ for the Kolmogorov cascade, $\alpha = 1/3$, which dominates the low-order structure functions, but approaches the Taylor microscale for $\alpha \approx 0$, in agreement with figure 9.

(*d*) There is another reason for structure functions not to behave as powers at small separations, and it results in a different limit for the self-similar behaviour. In standard multifractal theory, the structure function at separation R is dominated by structures of size R, but this is no longer true in the presence of structures whose volume does not scale as a power of their size. Consider S_p for separations such that

$R \gg \eta$, but small enough for their characteristic Kolmogorov velocity scale to be much smaller than u'. The statistics for velocity increments will receive a contribution of $O(u')$ whenever one of the ends of the measurement interval falls within one of the filaments, and the probability of that happening is proportional to their volume fraction. The contribution of the filaments to the mean is then $S_p^{(f)} \sim u'^p Re_\lambda^{-2}$, while the contribution from the rest of the flow is (Sreenivasan 1991)

$$S_p \sim u'^p (R/L_\epsilon)^{\zeta_p} \sim u'^p (RRe_\lambda^{-3/2}/\eta)^{\zeta_p}. \tag{5.16}$$

The contribution from the filaments dominates if

$$R_{p'} > \eta Re_\lambda^{3/2 - 2/\zeta_p}. \tag{5.17}$$

This length is within the inertial range if $\zeta_p > 4/3$ or $p > 4$, and tends to the integral scale when $\zeta_p \to \infty$. This implies that there should an intermediate range of scales between the dissipative and the inertial ranges in which all the structure functions above S_4 should tend to be independent of R, and that the extent of this range should be larger for the higher moments. The multifractal spectrum in figure 11(a) would be characteristic of the self-similar inertial range, while the isolated point would appear when considering scales in the intermediate region. The exponents for the two limits (5.15) and (5.17) are plotted in figure 11(b), using the scaling data from Sreenivasan (1991). For low-order functions, the first effect dominates, but the second scale becomes larger for $p > 4$. It should however be remembered that these results refer to scaling exponents, and that the ordering of the actual limiting separations may not be the same at any given finite Reynolds number.

In both cases there should be a Reynolds-number-dependent and order-dependent part of the inertial range in which the power scaling of the structure functions fails, and this effect should appear as a 'bump' of shallower slopes at the small-scale end of the high-order structure functions of high Reynolds number flows.

An early attempt to check this effect experimentally was made by van de Water, van der Vorst and van de Wetering (1991). More recently, Herweijer & van de Water (1995) have published very high-quality structure functions which show a clear bump near the end of the inertial range. Their conclusion is that the scale of the bump is independent of the Reynolds number, which would support the classical multifractal model, but it might be interesting to re-analyse their data in view of the predictions above.

6. Conclusions

We have confirmed the scalings obtained in JWSR for the properties of the most intense filaments in isotropic turbulence at $O(\eta)$ resolution. Their radii are of the order of a low multiple of the Kolmogorov scale and their azimuthal velocities are bounded by about 2.5 times the r.m.s. velocity of the flow. The former is explained because they are essentially Burgers' vortices in equilibrium with axial stretchings which are $O(\omega')$, of the same order as the background strain in the flow. No specially strong driving strains are needed to explain their origin. The stretching is inhomogeneous along the axes, compressive in many places, and with a correlation scale of the order of η, supporting the conclusion that it is essentially the turbulent background.

We have argued that this inhomogeneity explains the limit on the azimuthal velocity, following the arguments in VJO. Short filaments respond to variable stretching by developing axial pressure waves which weaken strongly stretched segments at the expense of the compressed ones, limiting the global maximum azimuthal velocity to

be of the same order as the total driving velocity difference, which is at most $O(u')$ in a turbulent flow. Stronger vortices become hollow and decay through a braiding instability of the resulting cylindrical vortex sheet. We have also suggested that the same waves connect initially short filaments into the observed long ones.

These two basic scalings can be combined to explain all the other local filament properties. In particular the axial vorticity scales as $\omega_0 \sim \omega_f = \omega' Re_\lambda^{1/2}$, and the internal Reynolds number of individual filaments is $\gamma/v \sim Re_\lambda^{1/2}$.

The last result suggests that filaments should become unstable for large Re_λ, and we have identified indirect evidence of this instability over a small fraction of the axial length, independent of Re_λ, along which the stretching is $O(\omega_f)$ and the radius is correspondingly thinner. If this is interpreted as a sign of self-stretching in the filaments, it implies kinking on the scale of the filament radius.

Extending this argument to a hierarchy of instabilities, which would act as long as the internal Reynolds number of the structures is large, we have shown that it would lead to a cascade of coherent filaments, in which the velocity increments are conserved, and whose limiting radius is $\eta_0 \approx v/u'$. If the resulting set is interpreted as deriving from the multifractal component for which the singularity exponent is $\alpha = 0$, its fractal dimension can be estimated as $D \approx 1$, which disagrees with the experimental result, $D(0) \approx 0$, in Sreenivasan (1991).

We have argued that this coherent cascade is only the strongest within a family, each of whose members is characterized by its own velocity scale. We have identified a region in the Δu–R classification of the turbulent fluctuations in which coherent structures are possible. It is roughly triangular (figure 9), with one vertex at the Kolmogorov scale, and the other two at $\Delta u \approx u'$ with $R \approx \eta_0$ and $R \approx \lambda$. The last point represents the thickest possible coherent filaments, which are also the ones with the weakest vorticity, and may correspond to some of the experimental observations by Cadot *et al.* (1995). This region would constitute a new scaling range, separating the self-similar multifractal inertial range from the dissipation limit. This would explain the observed discrepancy in the measured fractal dimensions.

We have noted that the existence of this range could be checked experimentally, and have suggested several possible tests in §5.4.

Another possible explanation of the discrepancy with the multifractal model is that the objects that we observe are artifacts of our relatively low Re_λ, and that we are only observing the initial stages of the instability cascade. Although our simulations contain a short range of approximately $k^{-5/3}$ energy spectrum, none of them has an inertial range in the classical sense that the Kolmogorov 4/5 law is satisfied (Jiménez 1997). The mean circulation of our vortices is only about $\gamma/v \approx 270$ at our highest Reynolds number, and it should be remembered that most of the hierarchy proposed in (5.2) would occur at lengths below our grid resolution. It has been reported by Tabeling *et al.* (1996) that beyond $Re_\lambda \approx 700$ ($\gamma/v \approx 530$) the distribution of the filament radius changes and that it becomes wider. Belin *et al.* (1996) also observe that, beyond that point, the flatness factor of the longitudinal velocity gradient stops increasing, but these observations have not been confirmed by other researchers (see Sreenivasan & Antonia 1997). Belin *et al.* (1997) have recently published a re-analysis of their data in which the transition at $Re_\lambda \approx 700$ appears as a temporary 'pause' in the growth of the flatness factor, rather than as a true upper limit.

The detected length of the filaments is proportional to the integral length of the flow L_ϵ, but we have identified a shorter correlation length which is $O(\lambda)$, although still much longer than the correlation length of the driving strain. It may be connected

with the origin of the filaments as instabilities of larger $O(\lambda)$ structures, as part of the coherent cascade mentioned above.

We have shown that the total volume fraction filled by filaments with axial vorticities above a fixed fraction of ω_f decreases as Re_λ^{-2}, but that this corresponds to a total length that increases as Re_λ. The vorticity contained in the filaments accounts for essentially all the strong vorticity in the flow above $\omega/\omega_f \approx 0.3$. Note that this behaviour of the volume fraction limits the relevance of the filaments to the dynamics of the flow. Since their characteristic velocities and vorticities are $O(u')$ and $O(\omega' Re_\lambda^{1/2})$, their total energy and enstrophy (or dissipation) decrease with Re_λ, respectively as Re_λ^{-2} and Re_λ^{-1}. In the high Reynolds number limit, both contributions become negligible. The lowest moment of the velocity gradients for which there is a contribution of the filaments which does not vanish at large Re_λ is the fourth-order flatness, and all the higher moments are eventually dominated by them. The effect of the coherent filaments on the different structure functions is further discussed in §5.4. The conclusion that the filaments contribute little to the total dissipation was tested directly in JWSR and has received strong support in an elegant recent experiment by Cadot, Bonn & Douady (1998) in which the filaments were suppressed by the addition of polymers, without any apparent effect on the energy dissipation.

Note that this picture is different from the early structural models of turbulence in which all the dissipation was assumed to be concentrated in the form of sheets (Corrsin 1962) or filaments (Tennekes 1968). In the present view the filaments, although responsible for most of the intermittency effects of the higher moments of the velocity derivatives, are themselves responsible for only a negligible part of the dissipation. A discussion of the differences between the two points of view can be found in the book by Frisch (1995, §8.9.2).

Appendix. Intersection probability between filaments

Assume a filament tangle of length $\ell_0 L_\epsilon^{-3}$ per unit volume. We are interested in its probability of approaching a 'test' segment of length $\mathrm{d}L$ within a distance D. Construct a cylinder whose axis is the test segment and whose base has area A. The projection of the tangle on the base of the cylinder is a line which, except for geometric factors of $O(1)$, has length $\ell_0 L_\epsilon^{-3} A \, \mathrm{d}L$. Construct a strip of width $2D$, centred on the projection of the tangle, which has area $\mathrm{d}S \sim 2D\ell_0 L_\epsilon^{-3} A \, \mathrm{d}L$. The tangle intersects the test segment if the strip contains the intersection of the test segment with the base of the cylinder, which happens with probability $\mathrm{d}S/A$. The probability of the tangle intersecting itself is therefore proportional to $D\ell_0^2 L_\epsilon^{-3}$ and, if each intersection perturbs the filament over a distance $O(D)$, the final perturbed fraction of the length would be

$$\ell_1/\ell_0 \sim (D/\ell_0)D\ell_0^2 L_\epsilon^{-3} = D^2 \ell_0/L_\epsilon^3. \tag{A 1}$$

Since we know from the discussion in §4 that $\ell_0 \sim L_\epsilon Re_\lambda$ and $D \sim \eta \sim L_\epsilon Re_\lambda^{-3/2}$, the perturbed fraction due to self-intersections of the tangle is

$$\ell_1/\ell_0 \sim Re_\lambda^{-2}, \tag{A 2}$$

which is negligible compared with the constant fraction that is found in (5.10). The implication is that the self-stretched segments described in §5 are due to vortex instabilities and not to intersections.

REFERENCES

ABRY, P., FAUVE, S., FLANDRIN, P. & LAROCHE, C. 1994 Analysis of pressure fluctuations in swirling turbulent flows. *J. Phys. Paris* II **4**, 725–733.

ANDREOTTI, B., COUDER, Y., DOUDAY, S. & MAURER, J. 1997 Experimental investigation of the turbulence near a large-scale vortex. *Euromech Colloq. 364, Carry-le-Rouet FR, June 1997. Eur. J. Mech.* B, in press.

ANSELMET, F., GAGNE, Y. & HOPFINGER, E. J. & ANTONIA, R. A. 1984 High order velocity structure functions in turbulent shear flows. *J. Fluid Mech.* **140**, 63–89.

BANDYOPADHYAY, P. R., STEAD, D. J. & ASH, R. L. 1991 Organised structure of a turbulent trailing vortex. *AIAA J.* **29**, 1627–1633.

BATCHELOR, G. K. 1953 *The Theory of Homogeneous Turbulence*. Cambridge University Press.

BELIN, F., MAURER, J., TABELING, P. & WILLAIME, H. 1996 Observation of intense filaments in fully developed turbulence. *J. Phys. Paris* II **6**, 573–583.

BELIN, F., MAURER, J., TABELING, P. & WILLAIME, H. 1997 Velocity gradient distributions in fully developed turbulence: experimental study. *Phys. Fluids* **9**, 3843–3850.

CADOT, O., BONN, D. & DOUADY, S. 1998 Turbulent drag reduction in a closed system: boundary layer versus bulk effects. *Phys. Fluids* **10**, 426–436.

CADOT, O., DOUADY, S. & COUDER, Y. 1995 Characterisation of the low-pressure filaments in a three-dimensional turbulent shear flow. *Phys. Fluids* **7**, 630–646.

CAMBON, C. & JACQUIN, L. 1989 Spectral approach to non-isotropic turbulence subject to rotation. *J. Fluid Mech.* **202**, 295–317.

CORRSIN, S. 1962 Turbulent dissipation fluctuations. *Phys. Fluids* **5**, 1301–1302.

DOUADY, S., COUDER, Y. & BRACHET, M. E. 1991 Direct observation of the intermittency of intense vorticity filaments in turbulence. *Phys. Rev. Lett.* **67**, 983–986.

HERWEIJER, J. & WATER, W. VAN DE 1995 Universal shape of scaling functions in turbulence. *Phys. Rev. Lett.* **74**, 4651–4654.

HOSOKAWA, I., OIDE, S. & YAMAMOTO, K. 1997 Existence and significance of 'soft worms' in isotropic turbulence. *J. Phys. Soc. Japan* **66**, 2961–2964.

FRISCH, U. 1995 *Turbulence: a Legacy of A. N. Kolmogorov*. Cambridge University Press.

FRISCH, U. & VERGASSOLA, M. 1991 A prediction of the multifractal model: the intermediate dissipation range. *Europhys. Lett.* **14**, 439–444.

JIMÉNEZ, J. 1992 Kinematic alignment effects in turbulent flows. *Phys. Fluids* A **4**, 652–654.

JIMÉNEZ, J. 1996 Algebraic probability density tails in decaying isotropic two-dimensional turbulence. *J. Fluid Mech.* **313**, 223–240.

JIMÉNEZ, J. 1997 Small-scale intermittency in turbulence. In *Euromech Colloq. 364, Carry-le-Rouet FR, June 1997. Euro. J. Mech.* B **17**, (1998) in press.

JIMÉNEZ, J. & WRAY, A. A. 1994a Columnar vortices in isotropic turbulence. *Meccanica* **29**, 453–464.

JIMÉNEZ, J. & WRAY, A. A. 1994b On the dynamics of small scale vorticity in isotropic turbulence. *CTR Ann. Res. Briefs* 1994, pp. 287–312.

JIMÉNEZ, J., WRAY, A. A., SAFFMAN, P. G. & ROGALLO, R. S. 1993 The structure of intense vorticity in isotropic turbulence. *J. Fluid Mech.* **255**, 65–90 (referred to herein as JWSR).

KAILASNATH, P., SREENIVASAN, K. R. & STOLOVITZKY, G. 1992 Probability density of velocity increments in turbulent flows. *Phys. Rev. Lett.* **68**, 2766–2769.

KUO, A. Y. & CORRSIN, S. 1972 Experiments on the geometry of the fine structure regions in fully turbulent fluid. *J. Fluid Mech.* **56**, 447–479.

NOULLEZ, A., WALLACE, G., LEMPERT, W., MILES, R. B. & FRISCH, U. 1997 Transverse velocity increments in turbulent flow using the RELIEF technique. *J. Fluid Mech.* **339**, 287–307.

PALADIN, G. & VULPIANI, A. 1987 Degrees of freedom of turbulence. *Phys. Rev.* A **35**, 1971–1973.

PARISI, G. & FRISCH, U. 1985 On the singularity structure of fully developed turbulence, in *Turbulence and Predictability in Geophysical Fluid Dynamics* (ed. M. Gil, R. Benzi & G. Parisi), pp. 84–88. North-Holland.

PASSOT, T., POLITANO, H., SULEM, P.-L., ANGILELLA, J. R. & MENEGUZZI, M. 1995 Instability of strained vortex layers and vortex tube formation in homogeneous turbulence. *J. Fluid Mech.* **282**, 313–338.

PORTER, D. H., WOODWARD, P. R. & POUQUET, A. 1998 Inertial range structures in decaying compressible turbulent flows. *Phys. Fluids* **10**, 237–245.

RASMUSSEN, H. 1995 The statistical theory of stationary turbulence. PhD Thesis, DAMTP, Cambridge University.

ROGALLO, R. S. 1981 Numerical experiments in homogeneous turbulence. *NASA Tech. Memo.* TM 81315.

SADDOUGHI, S. G. & VEERAVALI, S. V. 1994 Local isotropy in turbulent boundary layers at high Reynolds number. *J. Fluid Mech.* **268**, 333–372.

SAFFMAN, P. G. 1968 Lectures on homogeneous turbulence. In *Topics in Nonlinear Dynamics* (ed. N. J. Zabusky), pp. 485–614. Springer.

SAFFMAN, P. G. 1992 *Vortex Dynamics*, pp. 241–252. Cambridge University Press.

SIGGIA, E. D. 1981 Numerical study of small scale intermittency in three dimensional turbulence. *J. Fluid Mech.* **107**, 375–406.

SREENIVASAN, K. R. 1991 Fractals and multifractals in fluid turbulence. *Ann. Rev. Fluid Mech.* **23**, 539–600.

SREENIVASAN, K. R. & ANTONIA, R. A. 1997 The phenomenology of small-scale turbulence. *Ann. Rev. Fluid Mech.* **29**, 435–472.

TABELING, P., ZOCCHI, G., BELIN, F., MAURER, J. & WILLAIME, H. 1996 Probability density functions, skewness, and flatness in large Reynolds number turbulence. *Phys. Rev.* E **53**, 1613–1621.

TANAHASHI, M., MIYAUCHI, T. & IKEDA, J. 1997 Identification of coherent fine scale structure in turbulence. *Proc. IUTAM Symp. on Simulation and Identification of Organized Structures in Flows, Lyngby, Denmark, May 1997.*

TANAHASHI, M., MIYAUCHI, T. & MATSUOKA, K. 1997 Coherent fine scale structure in temporally developing turbulent mixing layers. *Proc. 2nd Intl Symp. on Turbulent Heat and Mass Transfer*, (ed. K. Hanjalic & T. W. Peeters) Delft, The Netherlands, June 9–12, 1997, pp. 461–470.

TENNEKES, H. 1968 Simple model for the small-scale structure of turbulence. *Phys. Fluids* **11**, 669–671.

VASSILICOS, J. C. & BRASSEUR, J. G. 1996 Self-similar spiral flow structure in low Reynolds number isotropic and decaying turbulence. *Phys. Rev.* E **54**, 467–485.

VERZICCO, R. & JIMÉNEZ, J. 1997 On the survival of vortex filaments in turbulence. *Euromech Colloq. 364, Carry-le-Rouet FR, June 1997.* Submitted *J. Fluid Mech.*

VERZICCO, R., JIMÉNEZ, J. & ORLANDI, P. 1995 Steady columnar vortices under local compression. *J. Fluid Mech.* **299**, 367–388 (referred to herein as VJO).

VILLASENOR, J. & VINCENT, A. 1992 An algorithm for the space recognition and time tracking of vorticity tubes in turbulence. *CVGIP: Image Understanding* **55**, 27–35.

VILLERMAUX, E., SIXOU, B. & GAGNE, Y. 1995 Intense vortical structures in grid-generated turbulence. *Phys. Fluids* **7**, 2008–2013.

VINCENT, A. & MENEGUZZI, M. 1991 The spatial structure and statistical properties of homogeneous turbulence. *J. Fluid Mech.* **225**, 1–20.

VINCENT, A. & MENEGUZZI, M. 1994 On the dynamics of vorticity tubes in homogeneous turbulence. *J. Fluid Mech.* **258**, 245–254.

WATER, W. VAN DE, VORST, B. VAN DER & WETERING, E. VAN DE 1991 Multiscaling of turbulent structure functions. *Europhys. Lett.* **16**, 443–448.

WRAY, A. A. 1997 A numerical simulation of decaying isotropic turbulence. In *A Data Base for the Validation of LES Computations in Transition and Turbulence* (ed. J. Jiménez), *AGARD R-345*, data set HOM02.

ZEMAN, O. 1994 A note on the spectra and decay of rotating homogeneous turbulence. *Phys. Fluids* **6**, 3221–3223.

ZEMAN, O. 1995 The persistence of trailing vortices: A modelling approach. *Phys. Fluids* **7**, 135–143.